012539-2-F

PERFORMANCE OF ATCRBS LOCATED ABOVE A FLAT GROUND WITH VARIABLE DIELECTRIC CONSTANT

Dipak L. Sengupta

ABSTRACT

The SLS mode performance of ATCRBS located above a flat ground with variable dielectric constant is theoretically investigated. It is found that at the ATCRBS frequency the effects of loss in the ground may be neglected in most of the cases. The increase of the dielectric constant tends to smooth out the oscillations around the free space values of all the quantities characterizing the ATCRBS performance. The performances of ATCRBS using the existing Hog-trough and the Hazeltine open array antenna have been studied. It is found that the ATCRBS performance with the former antenna is more sensitive to the variations of the dielectric constant. This implies that antennas with large field gradient will be less sensitive to the dielectric constant variations due to weather and general environmental changes.

key words:

SLS mode ATCRBS performance
effects of variable dielectric constant
coverage patterns
vertical lobing
mainbeam killing
sidelobe 'punch through'

MISSING PAGE

PREFACE

The report investigates theoretically the effects of variations in the dielectric constant of ground on the SLS mode performance of ATCRBS located above a flat ground. In general it is found that a large value of dielectric constant of ground smoothes out the oscillations in the various quantities characterizing the ATCRBS performance. It is also found that the sensitivity of ATCRBS performance to dielectric constant variations of ground is less if the interrogation antenna system possesses larger field gradient.

MISSING
PAGE

TABLE OF CONTENTS

LIST OF ILLUSTRATIONS

LIST OF TABLES

1. INTRODUCTION

The results of a theoretical study of ATCRBS located above a perfectly dielectric flat ground have been reported earlier[1 - 3]. In the present report we consider the ground to have both real and complex values of the dielectric constant and study their effects on ATCRBS performance. Specifically we study the SLS mode performance of ATCRBS using the Hazeltine open array and the existing Hog-trough antennas to radiate the interrogation signals. The results of the present study may be found useful in estimating the sensitivities of various ATCRBS antennas and hence of the ATCRBS performance to changes in the ground constants due to weather and other environmental changes

2. GROUND REFLECTION COEFFICIENT

In order to account for the loss associated with the ground we assume that its dielectric constant is complex. With assumed time dependence $e^{j\omega t}$, the appropriate form for the complex dielectric constant is given by:

$$\epsilon_c = \epsilon_r - j\frac{\sigma}{\omega\epsilon_0} = \epsilon_r - j\frac{18 \times 10^3 \sigma}{f_{MHz}} \quad , \tag{1}$$

where

ϵ_r is the usual dielectric constant of ground,

σ is the conductivity of ground in mhos/meter

$\epsilon_0 = \frac{1}{36\pi} \times 10^{-9}$ farad/meter = permittivity of free space,

ω is the frequency in radians

f_{MHz} is the frequency in megahertz

Let us consider a horizontally oriented interface between free space and a flat ground. The reflection coefficient for vertically polarized plane electromagnetic waves incident at the interface from the free space side is given by [4, 5] :

$$\Gamma = \rho e^{-j\phi} = \frac{\epsilon_c \sin\theta - \sqrt{\epsilon_c - \cos^2\theta}}{\epsilon_c \sin\theta + \sqrt{\epsilon_c - \cos^2\theta}} \quad , \tag{2}$$

where

Γ is the complex reflection coefficient,

ρ and ϕ are the magnitude and the lagging phase angle of Γ, respectively,

θ is the angle of incidence measured from the horizon.

From Eq. (2) it is found that for real dielectric constant, i.e., $\epsilon_c = \epsilon_r$, the reflection coefficient goes to zero for the critical incident angle θ_B given by

$$\theta_B = \sin^{-1}\left(\frac{1}{\sqrt{\epsilon_{r+1}}}\right) \quad . \tag{3}$$

In our notation the critical angle θ_B is the complement of the usual Brewster angle

[4]. When θ is less than θ_B, $\phi = \pi$, but at $\theta = \theta_B$ it decreases abruptly to zero where it remains for all values of $\theta > \theta_B$.

When the dielectric constant is complex, ρ can decrease only to a minimum value greater than zero, reaching the minimum at an angle smaller than that given by Eq. (3). At the same time for complex ϵ_c, ϕ is no longer discontinuous at this angle, but decreases rapidly from somewhat less than π to a small value and decreases slowly thereafter. As ϵ_c becomes very large, the critical angle approaches zero, the minimum value of ρ approaches unity, i.e., $\rho \longrightarrow +1$ for all values of θ.

Figure 1(a) shows the magnitude of the reflection coefficient as a function of θ, for four values of the complex dielectric constant such that the real parts of ϵ_c are kept constant at 3 and the imaginary parts are varied as shown. The three values of the imaginary parts of ϵ_c, 0.5, 1.5 and 3.0 correspond at 1030 MHz to the conductivities σ of 28.6, 85.8 and 171.6 millimhos respectively. For a medium having $\epsilon_r = 3$ these are rather large values for σ and may not be realistic—they are assumed here to bring out the effects of loss. The corresponding variations of the phase angle of the reflection coefficients are shown in Fig. 1(b). The results shown in Figs. 1 indicate that at the operating frequency of ATCRBS, for a medium having dielectric constant $\epsilon_r = 3$ the assumed values of conductivity do not appreciably alter the values of ρ in the range $0 \leq \theta \leq 10^o$ than those of the lossless case, but affects the values of ϕ slightly. This would imply that the positions of the lobes in the P1 - P2 patterns produced by the ATCRBS antenna located above such a lossy medium will be slightly different than the lossless case, but their amplitudes will be approximately the same with $0 \leq \theta \leq 10^o$.

As mentioned earlier, for real dielectric constant the magnitude of the reflection coefficient varies monotonically as $1 \leq \rho \leq 0$ in the range $0 \leq \theta \leq \theta_B$; for $\theta > \theta_B$, ρ again increases monotonically and assumes a maixmum value of $\sqrt{\epsilon_r} - 1/\sqrt{\epsilon_r} + 1$ at $\theta = \pi/2$. The variation of the critical angle as a function of the dielectric constant (ϵ_r) is shown in Fig. 2. Figure 3 shows ρ vs. θ for three large values of the real dielectric constant. The values of the critical angles corresponding to each medium are indicated by the arrows on the abscissa of Fig. 3. From the point of view of ATCRBS performance it is important to observe that for $\theta < \theta_B$, ρ decreases rapidly to zero at the critical angle; also in this range ρ is smaller for larger ϵ_r. As a result of this, within this range of θ the amplitudes

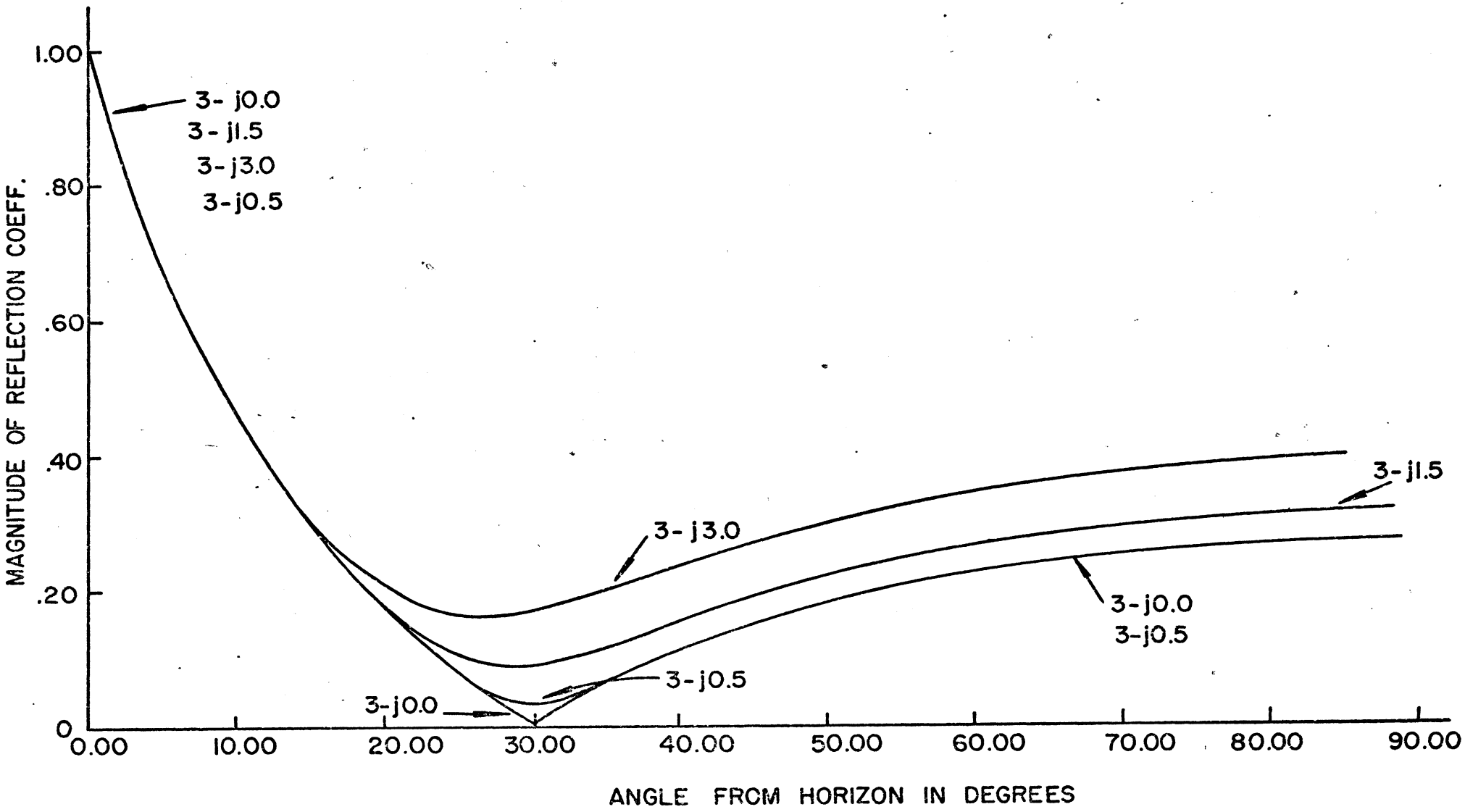

FIG. 1(a): Magnitude of the reflection coefficient as a function of the incident angle with the imaginary part of the complex dielectric constant as the parameter.

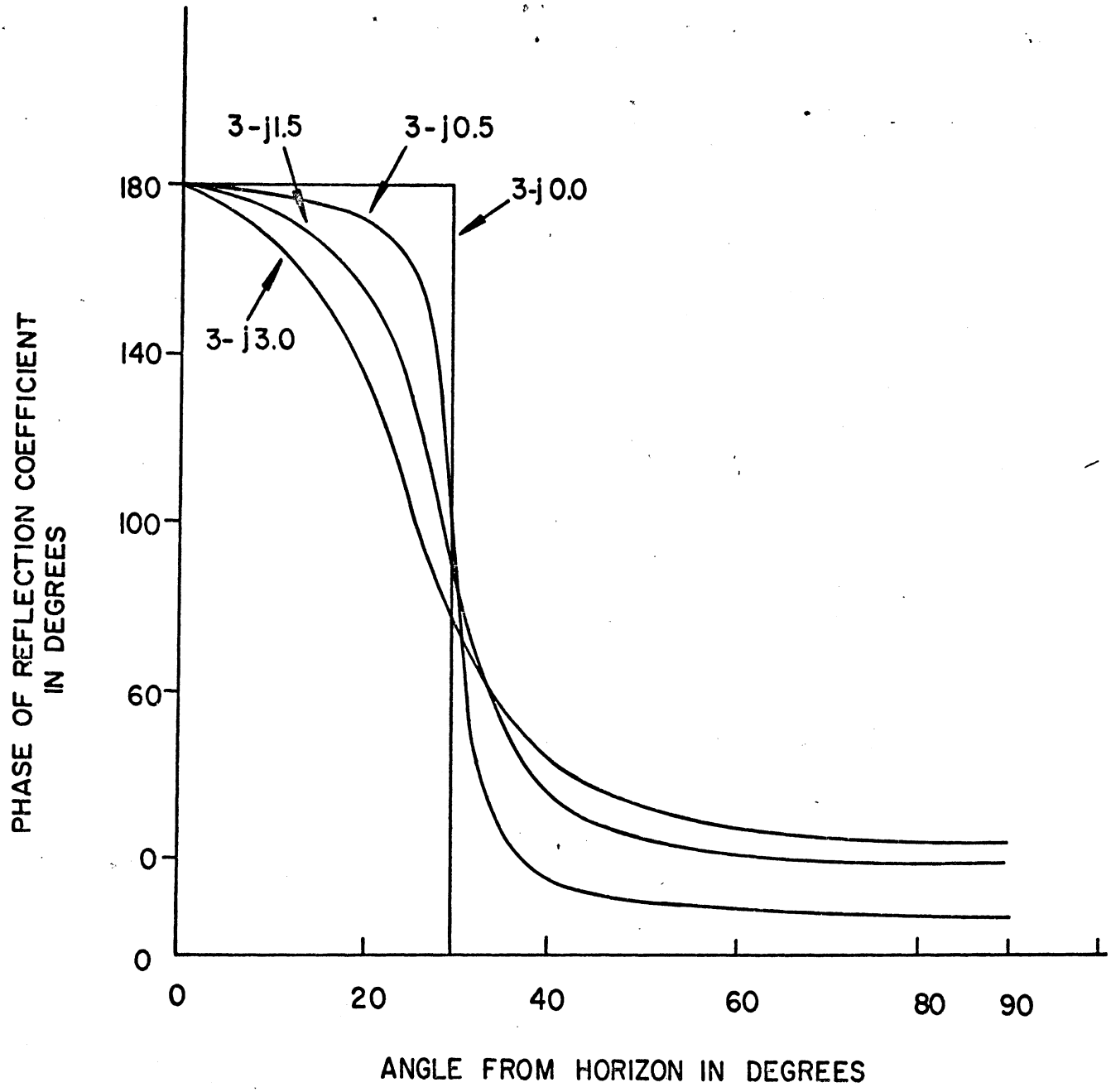

FIG. 1(b): The phase of the reflection coefficient as a function of the incident angle with the imaginary part of the complex dielectric constant as the parameter.

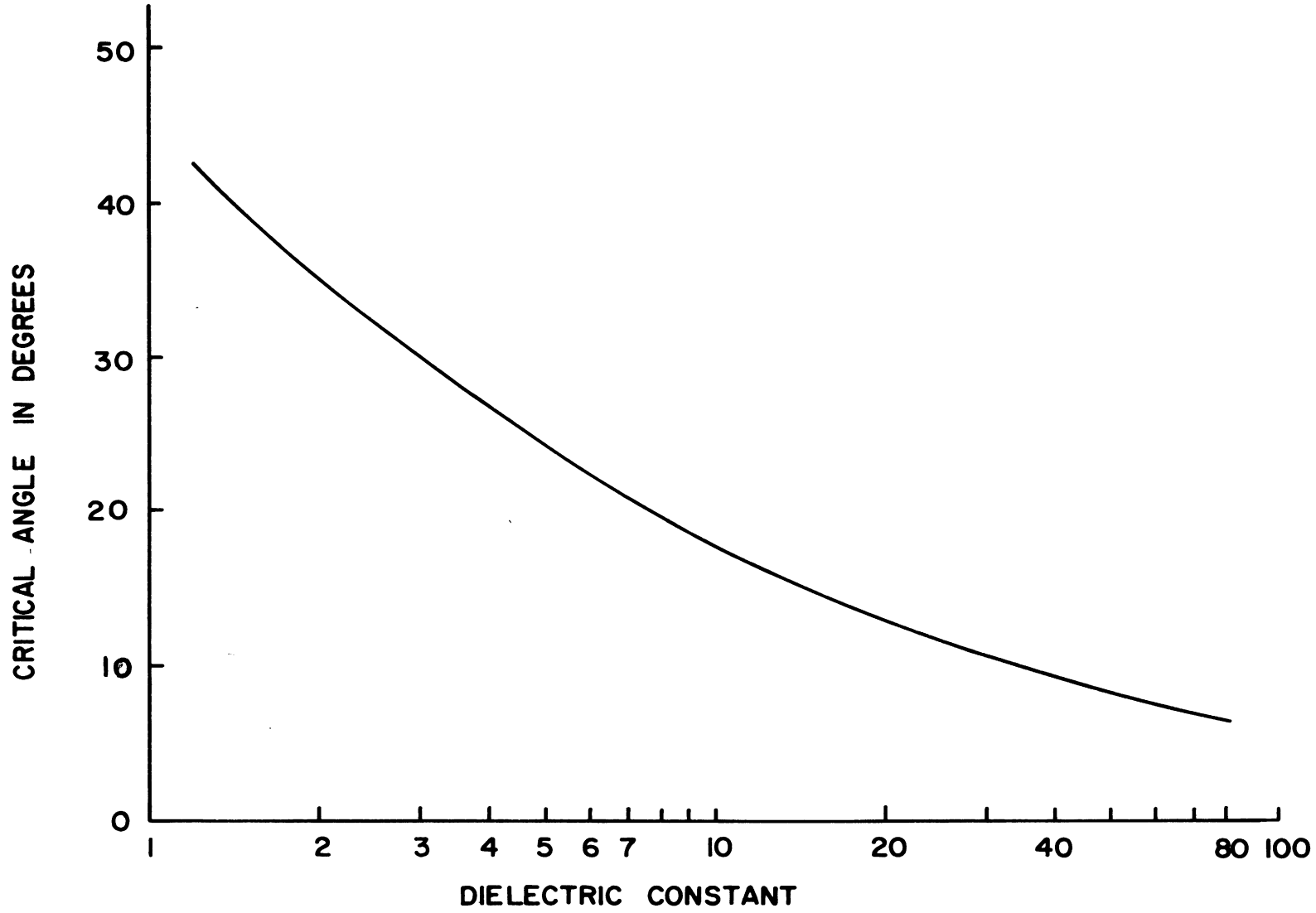

FIG. 2: Critical angle (θ_B) as a function of the dielectric constant (ϵ_r).

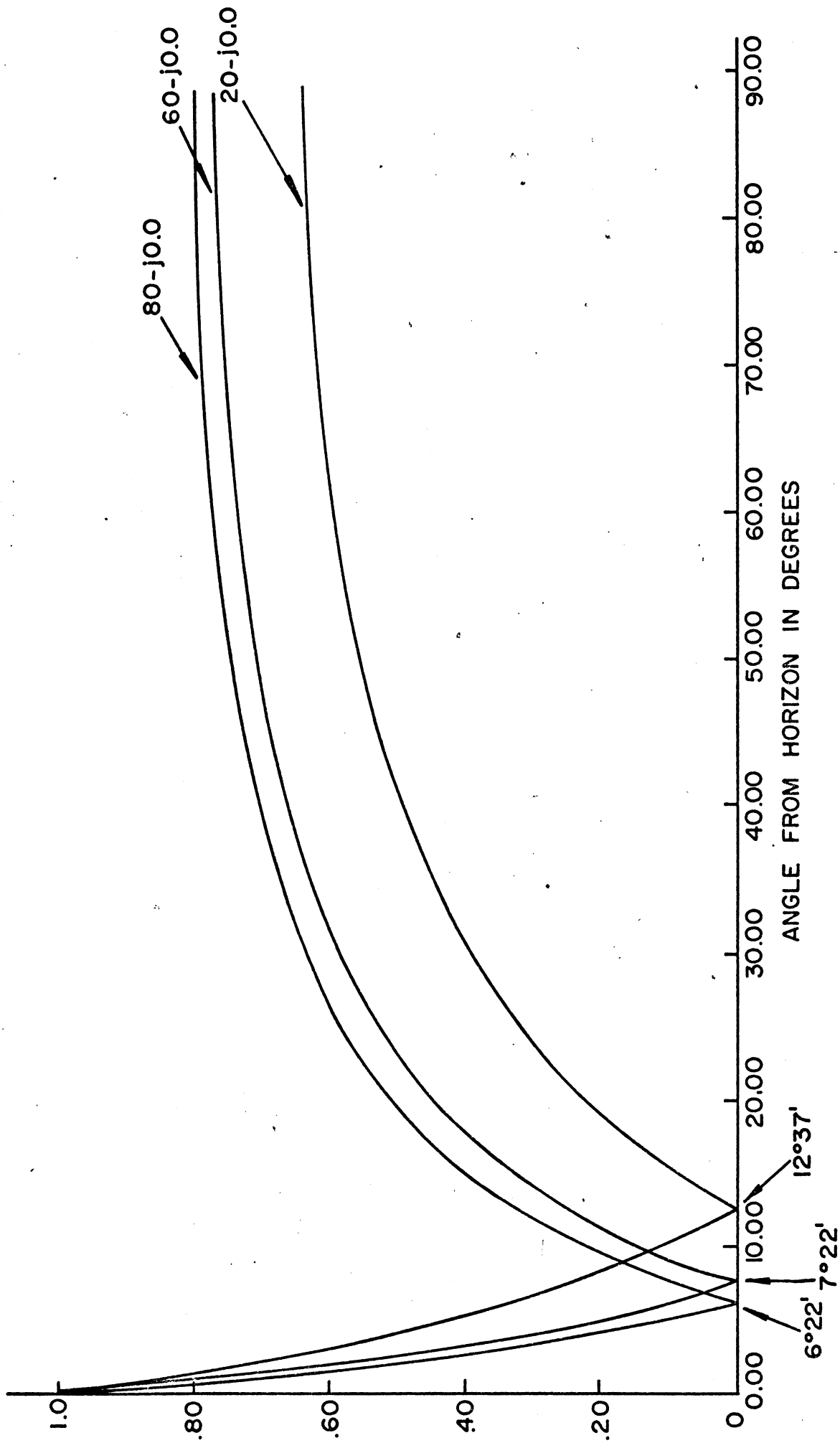

FIG. 3: Magnitude of the reflection coefficient as a function of the incident angle with the dielectric constant (ϵ_r) as the parameter. Arrows show the corresponding critical angles.

of the maxima and the depths of the minima in the P1 - P2 lobing patterns will decrease as ϵ_r is increased. For $\theta > \theta_B$, ρ is larger for larger ϵ_r and hence the behavior of the amplitudes of maxima and the depths of the minima as functions of ϵ_r will be the reverse.

Typical values of the dielectric constant ϵ_r and conductivity of σ some representative media are shown in Table I, which is taken from [6] where the detailed variations of ρ and ϕ for these media are also given. The corresponding values of the imaginary part ϵ_i of the complex dielectric constant at f = 1030 MHz are also shown in Table I. From the results shown, it is found that at the ATCRBS frequency the effects of loss may be neglected in most of the cases. In the case of snow the real and imaginary parts of ϵ_c are of the same order and hence should be considered for better accuracy of the final results. Even with high loss, as shown in Fig. 1, within the region of interest to ATCRBS,, say $0^o \leq \theta \leq 10^o$, the effects of loss caused by the variations of ρ on the lobing pattern may be assumed to be negligible.

Table 1
Dielectric constants and conductivities of some representative media [6] .

Type	ϵ_r	σ mhos/m	f = 1030 MHz
Fresh snow	1.2	0.070	1.225
Packed snow	1.5	0.600	10.500
Dry turf with short grass	3	0.050	0.875
City industrial area	5	0.001	0.018
Wet truf with short short grass	6	0.100	1.750
Rocky soil dry	14	0.002	0.035
Rocky soil, 10 percent moisture	30	0.002	0.035
Fresh water	81	0.010	0.175
Sea water	80	3	52.5

3. ATCRBS ANTENNAS

It is assumed that the ATCRBS uses the existing Hog-trough and Hazeltine open array antennas to radiate the interrogating signals. The free space pattern characteristics of these two antennas are described in [1] and will not be repeated here. The measured antenna characteristics of interest for the present purpose are shown in Table 2 [7] .

Note that the Hazeltine antenna pattern has a field gradient which is about three times larger than that of the existing Hog-trough antenna. As a result of this, the lobings in the pattern produced by the exisitng antenna will continue over a larger region of space. In the following sections we discuss the various quantities characterizing the performance of ATCRBS using the above two antennas located above a flat ground having variable dielectric constant. The theoretical basis for obtaining the numerical results given below is similar to that described in [1] .

Table 2
Measured characteristics of ATCRBS antennas at 1030 MHz [7].

Gain (over isotropic)	23 dB	21 dB
Horizontal beamwidth (3 dB)	2.45^{o}	2.35^{o}
Vertical beamwidth (3 dB)	29^{o}	50^{o}
Field gradient (elevation pattern roll-off) at -6 dB	1.14 dB/deg.	0.37 dB/deg.
Azimuth plane sidelobes	-25 dB	-25 dB
Horizontal aperture	26 ft	27 ft
Elevation aperture	4 ft	21 in

4. RESULTS FOR HAZELTINE OPEN ARRAY ANTENNA

Figures 4(a) and 4(b) show the SLS mode P1 and P2 pulse patterns obtained with the Hazeltine antenna located above ground having dielectric constant equal to 3 and 80 respectively. For reference the free space P1 and P2 patterns are also shown in Figs. 4(a) and 4(b). It is found from the results that the lobings in the pattern smooth out at $\theta > 10^{o}$ for $\epsilon_c = 3.0 - j0.0$ and at $\theta > 5^{o}$ for $\epsilon_c = 80 - j0.00$. In general, increase of the dielectric constant tends to smooth out the patterns. This can be seen more clearly from Fig. 5 where the P1 and P2 patterns for $\epsilon_c = 3 - j0.00$ and $80 - j0.00$ are shown on the same plot on an expanded scale in the range $0 \leq \theta \leq 5^{o}$. It is clear from Fig. 5 that with larger dielectric constant the amplitudes of the maxima and the depths of the minima are reduced.

Fig. 6(a) and 6(b) show the corresponding SLS mode normalized pulse ratio patterns, i.e., P1/P2 vs. θ. The results indicate that the variations of P1/P2 continue over a larger range of θ for smaller ϵ_c and that the amplitudes of variations are smaller for larger ϵ_c. The normalized pulse ratios assumes zero values at $\theta \simeq 7^{o}10'$ and $14^{o}15'$ respectively; these angles are determined by the separation distance between the phase centers of the directional and omnidirectional antennas. This will be discussed in further detail later. Note that in Fig. 6(b) the critical angle is $6^{o}22'$ where the pulse ratio also assumes zero value. The mainbeam killing and sidelobe punch-through threshold levels for the antenna are also shown in Fig. 6 assuming that the two levels at the transponder are 9 dB and 0 dB respectively. For better comparison, Fig. 7 shows the two pulse ratio patterns on the same plot on an expanded scale in the range $0 \leq \theta \leq 5^{o}$. It is found from the results that the large dielectric constant completely eliminates the mainbeam killing and sidelobe punch-through zones.

In order to bring out the effects of ground conductivity we consider the pulse and pulse ratio patterns when $\epsilon_c = 80 - j52.5$ as shown in Figs. 8(a) and 8(b). These results should be compared with Figs. 4(b) and 6(b) respectively. From the results it may be concluded that in the present case for the amount of loss assumed in the medium the two results are not appreciably different.

Figures 9(a) and 9(b) show the number of replies as function of θ for $\epsilon_c = 3 - j0.00$ and $\epsilon_c = 80 - j0.00$ respectively within the range $0 \leq \theta \leq 5^{o}$. The most significant

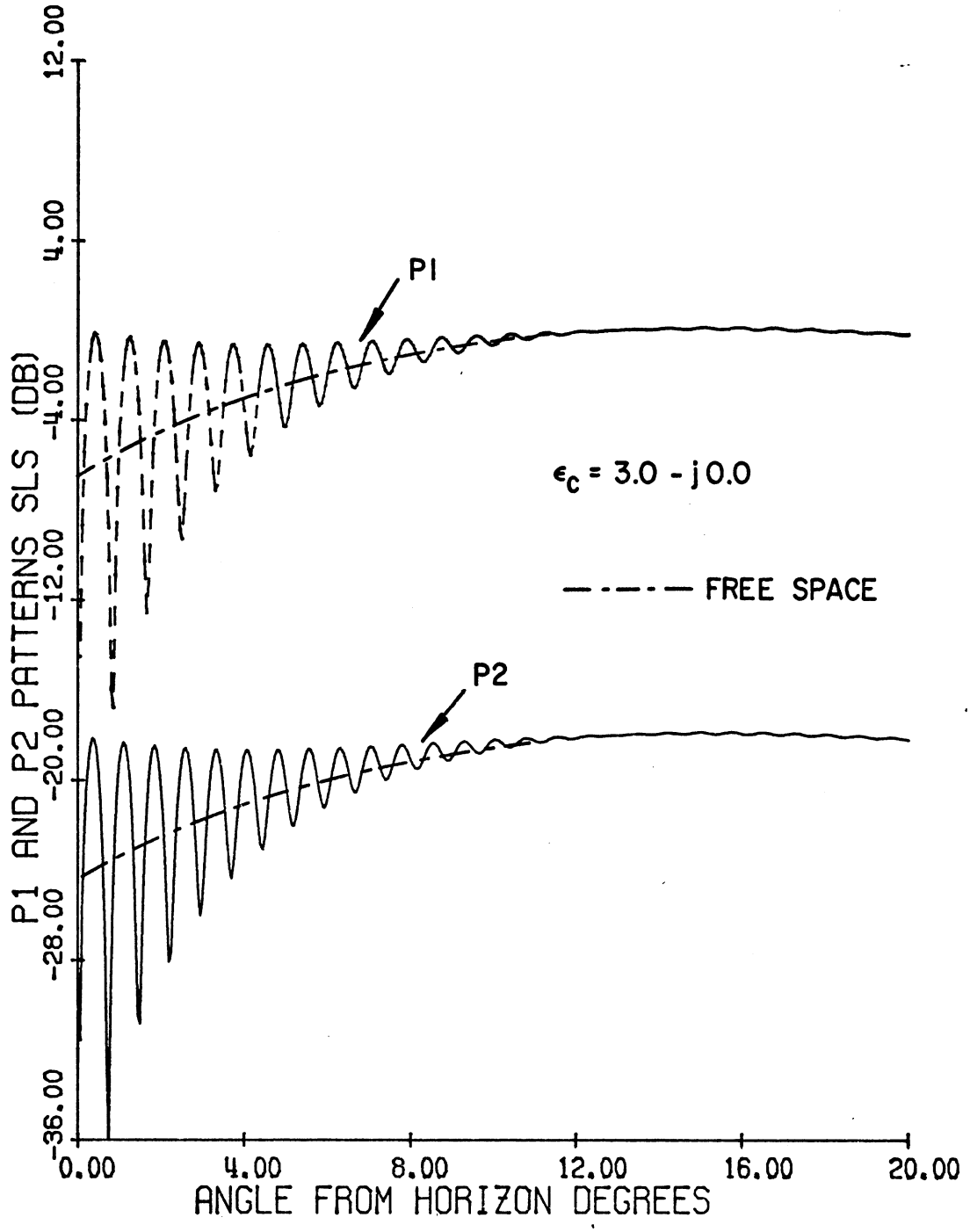

FIG. 4(a): SLS mode P1 and P2 pulse patterns for the Hazeltine antenna. $\epsilon_r = 3.$

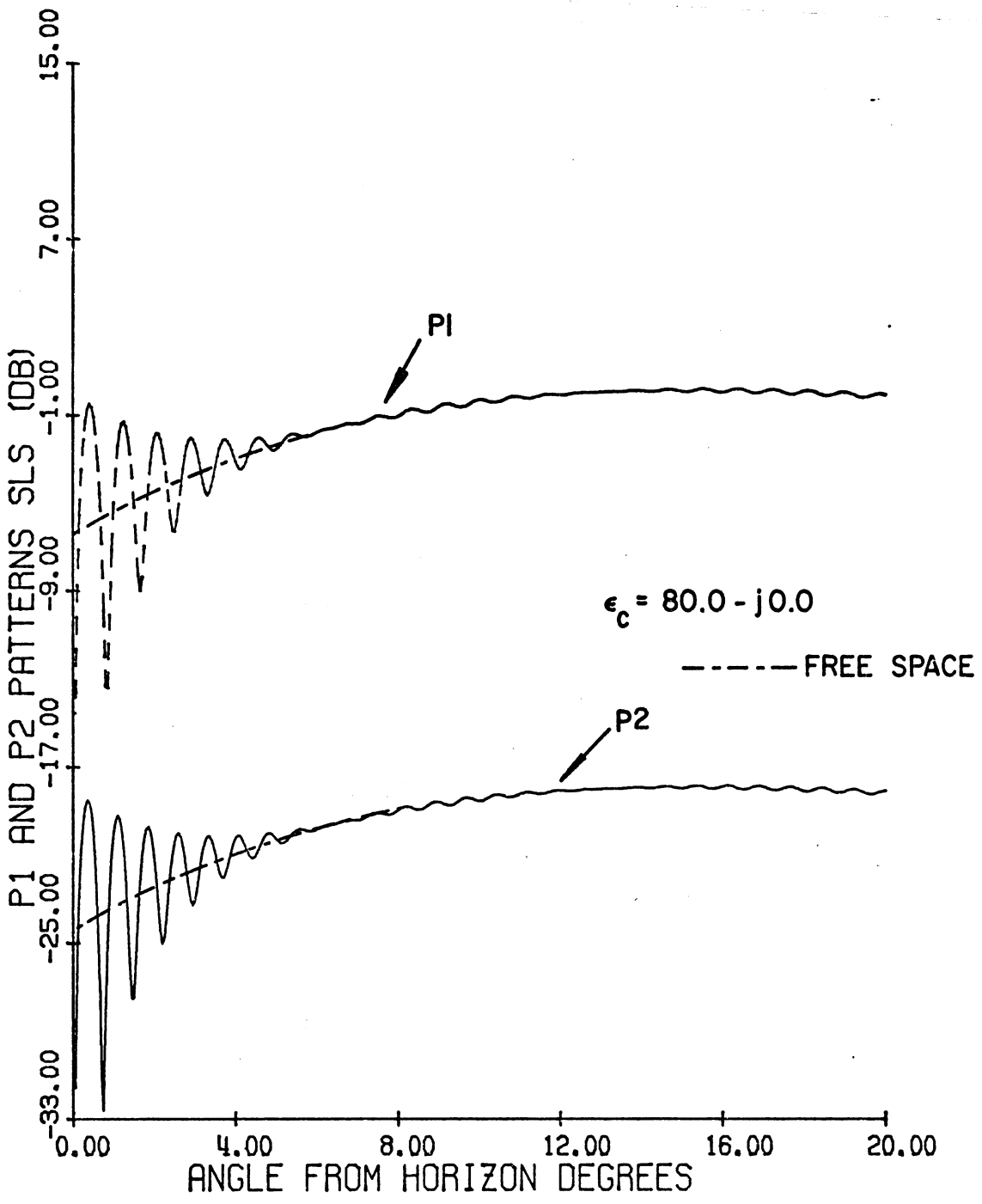

HAZELTINE ANTENNA TILTED ANGLE= 0.0 D
ELEV.: DIREC. 33.00' OMNI. 37.00'
P1/P2= 18.00 DB.

FIG. 4(b): SLS mode P1 and P2 pulse patterns for the Hazeltine antenna. $\epsilon_r = 80.0$.

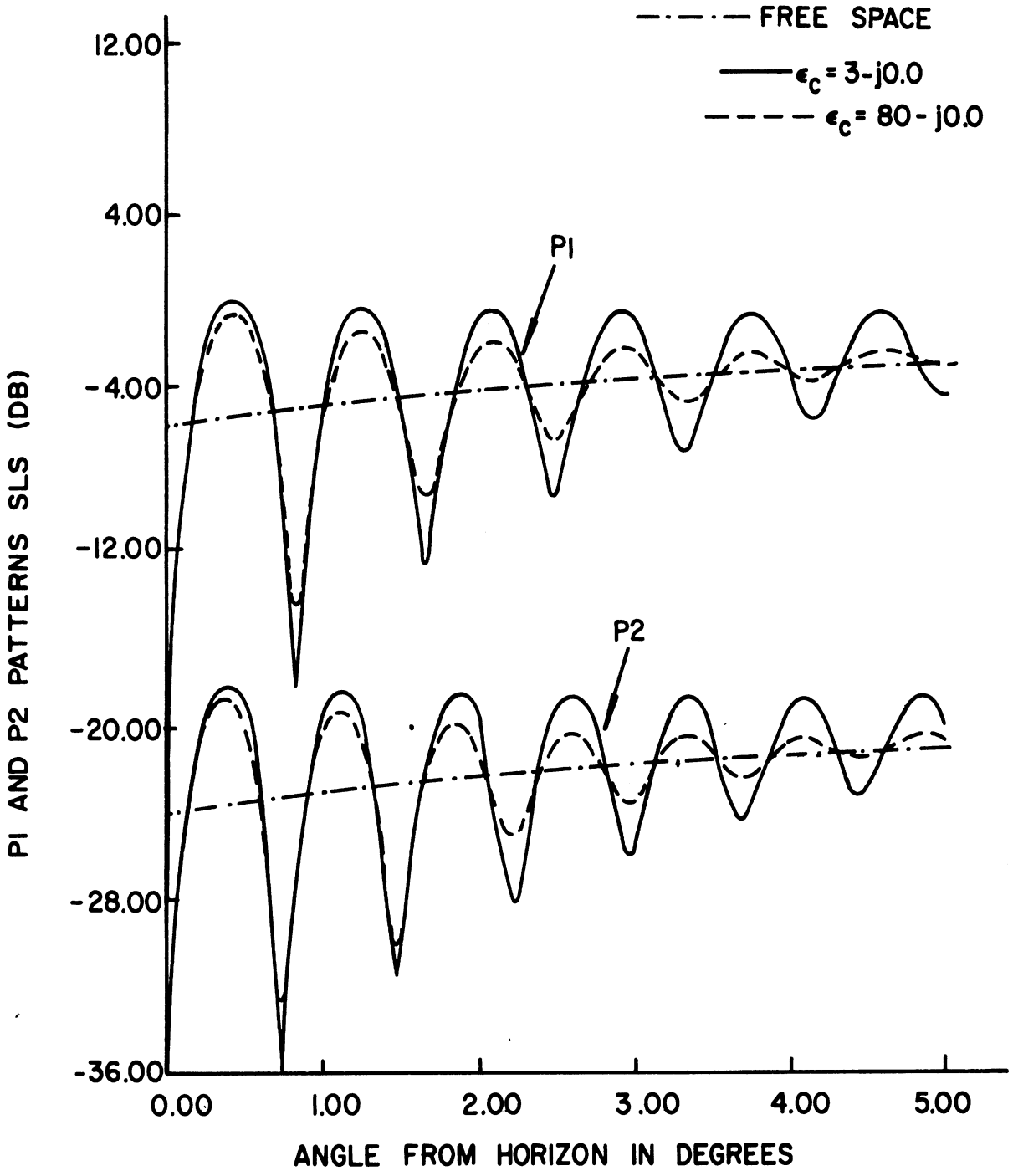

FIG. 5: SLS mode P1 and P2 pulse patterns on expanded scale for the Hazeltine antenna.

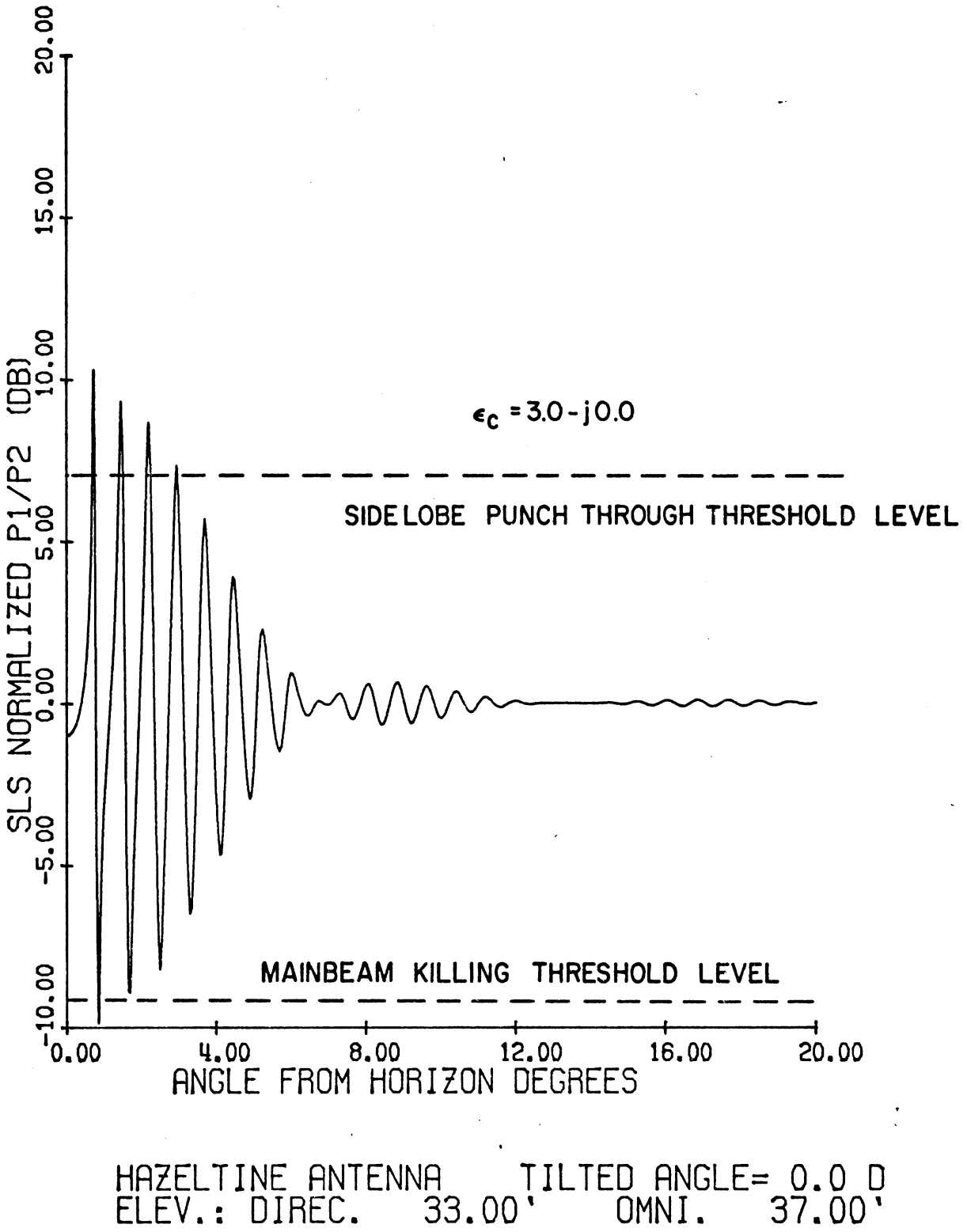

FIG. 6(a): SLS mode normalized pulse ratio pattern for the Hazeltine antenna. $\epsilon_r = 3.0$.

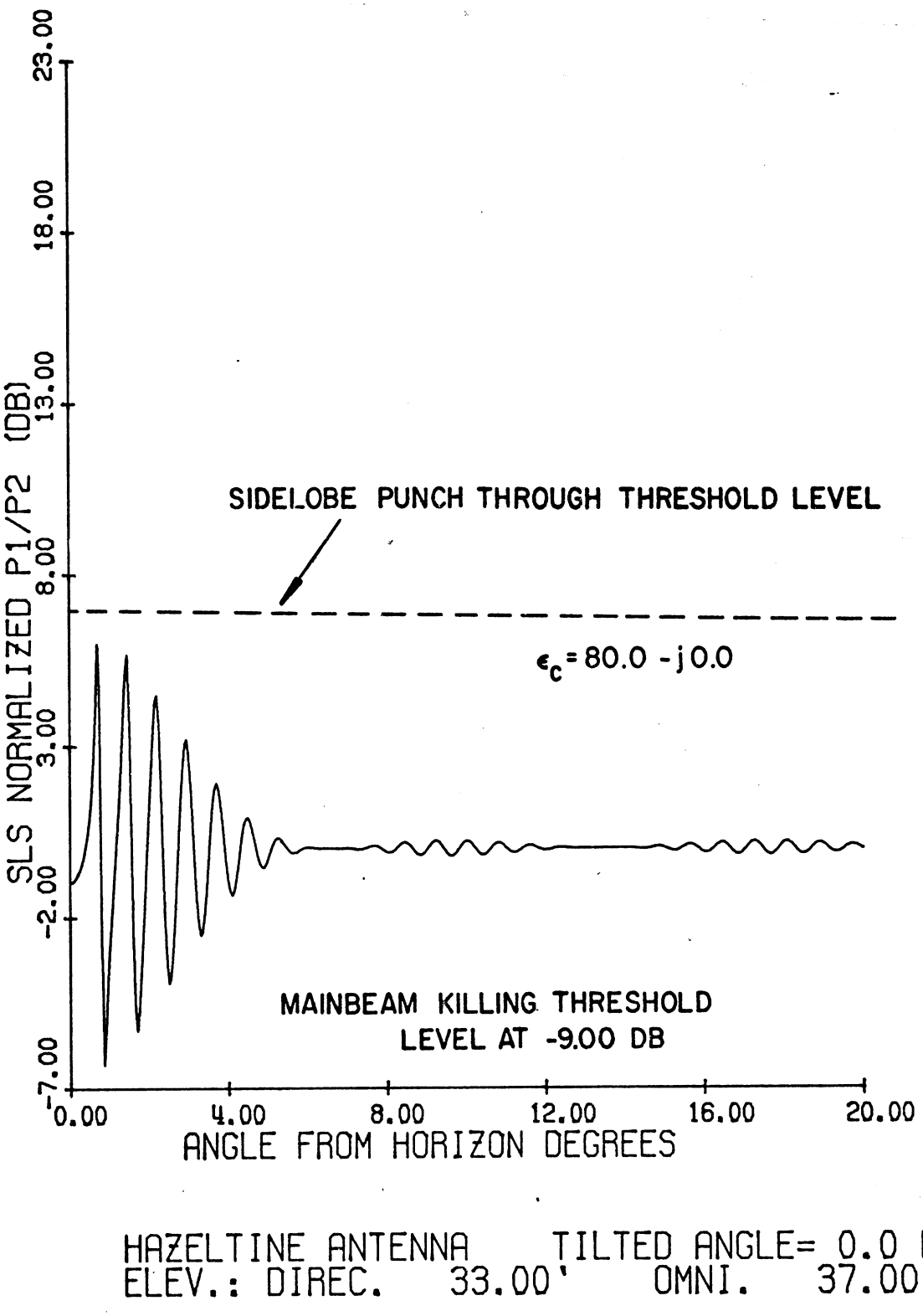

FIG. 6(b): SLS mode normalized pulse ratio pattern for the Hazeltine antenna. $\epsilon_r = 80.0$.

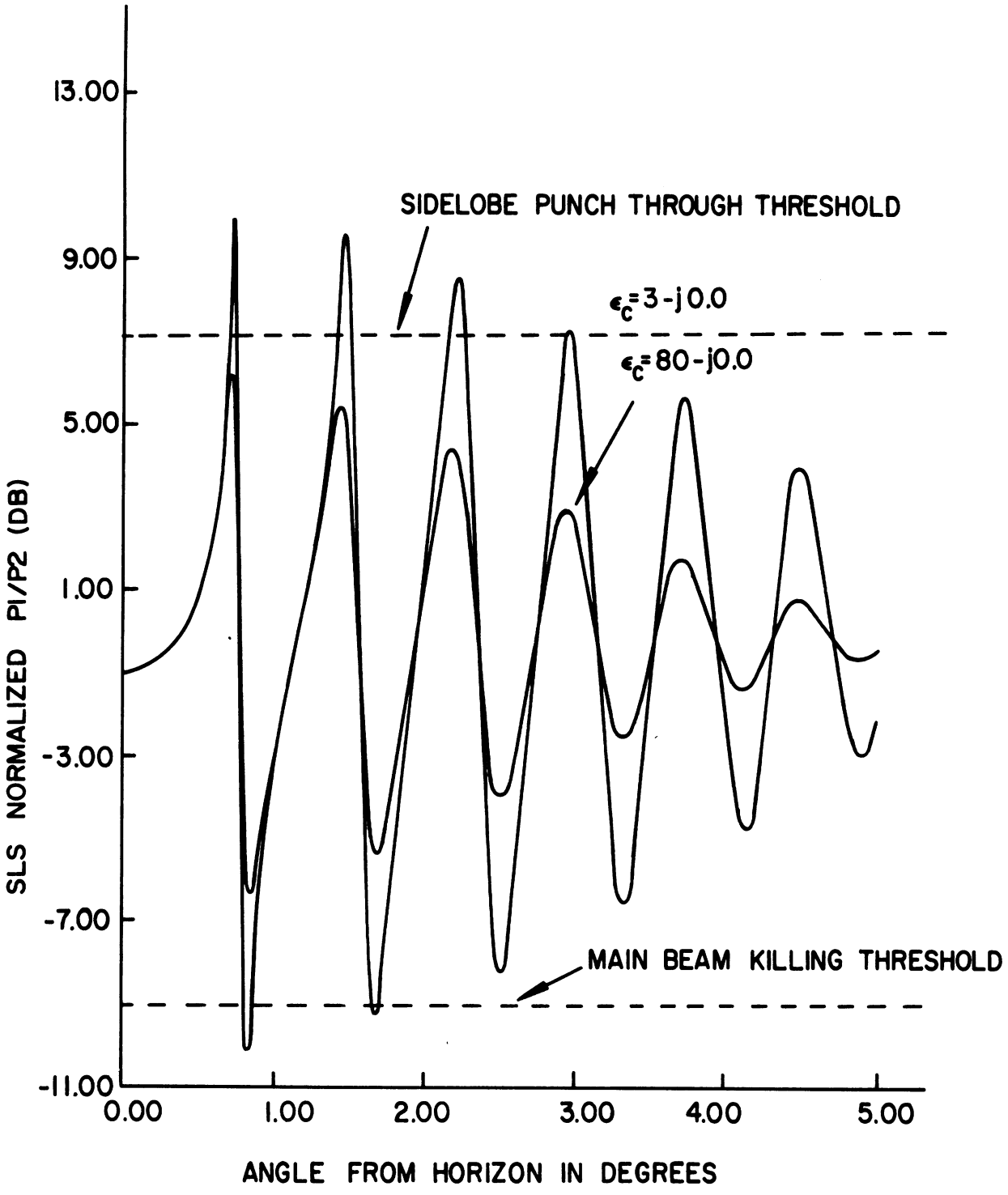

FIG. 7: SLS mode normalized pulse ratio patterns on an expanded scale for the Hazeltine antenna.

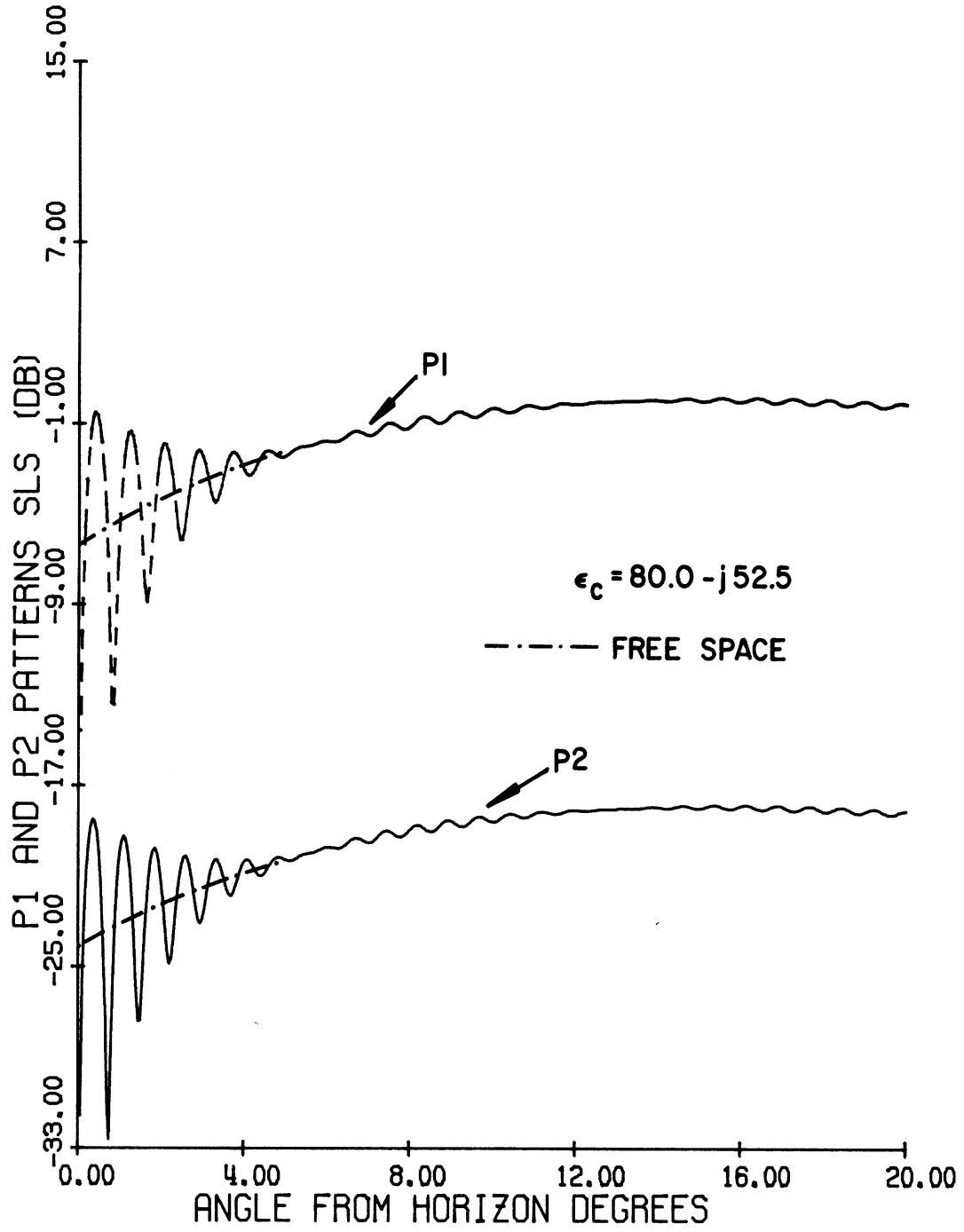

HAZELTINE ANTENNA TILTED ANGLE= 0.0 D
ELEV.: DIREC. 33.00' OMNI. 37.00'
P1/P2= 18.00 DB.

FIG. 8(a): SLS mode P1 and P2 pulse pattern for the Hazeltine antenna. ϵ_c = 80.0 - j52.5.

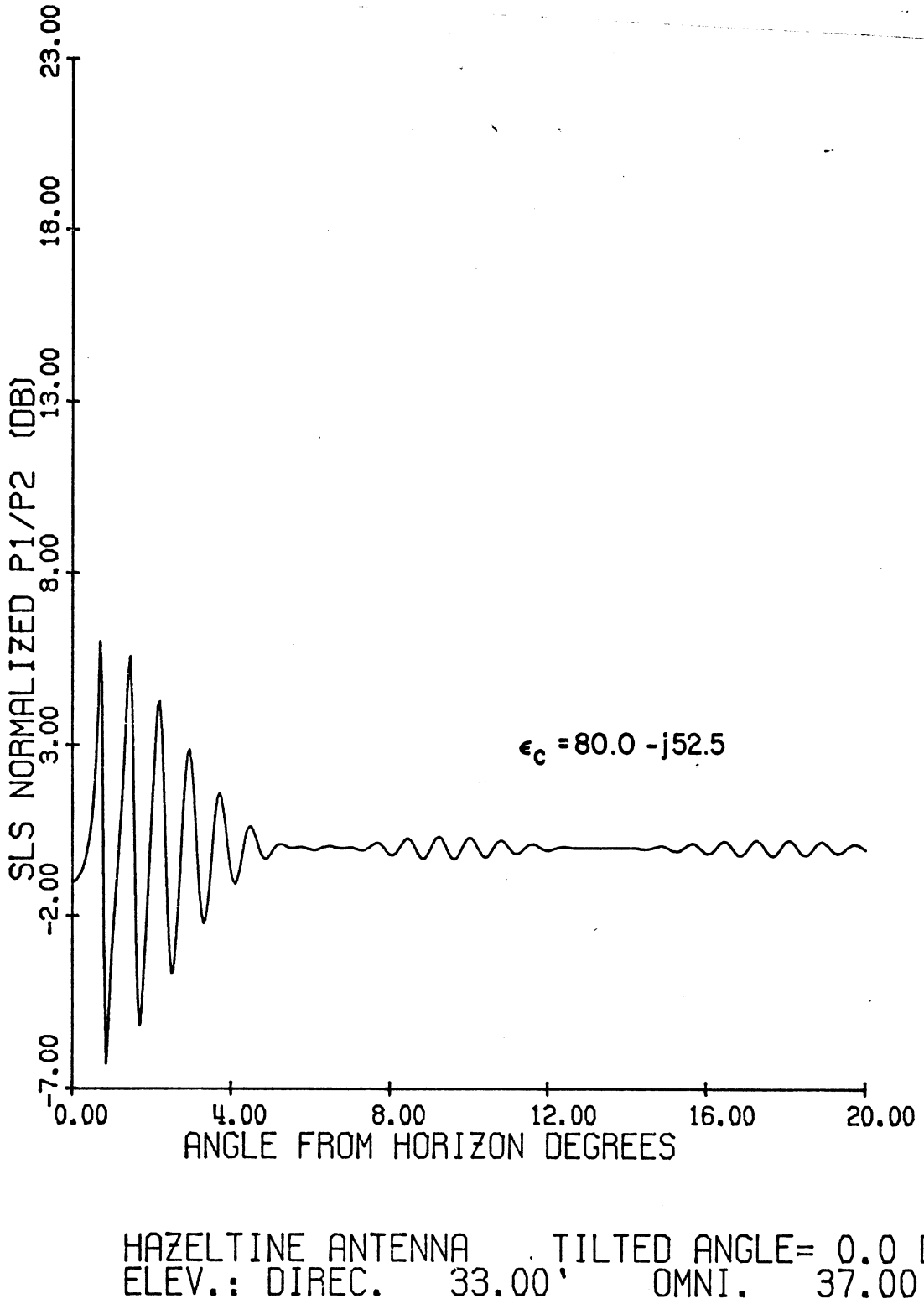

FIG. 8(b): SLS mode normalized pulse ratio pattern for the Hazeltine antenna. $\epsilon_c = 80.0 - j52.5$.

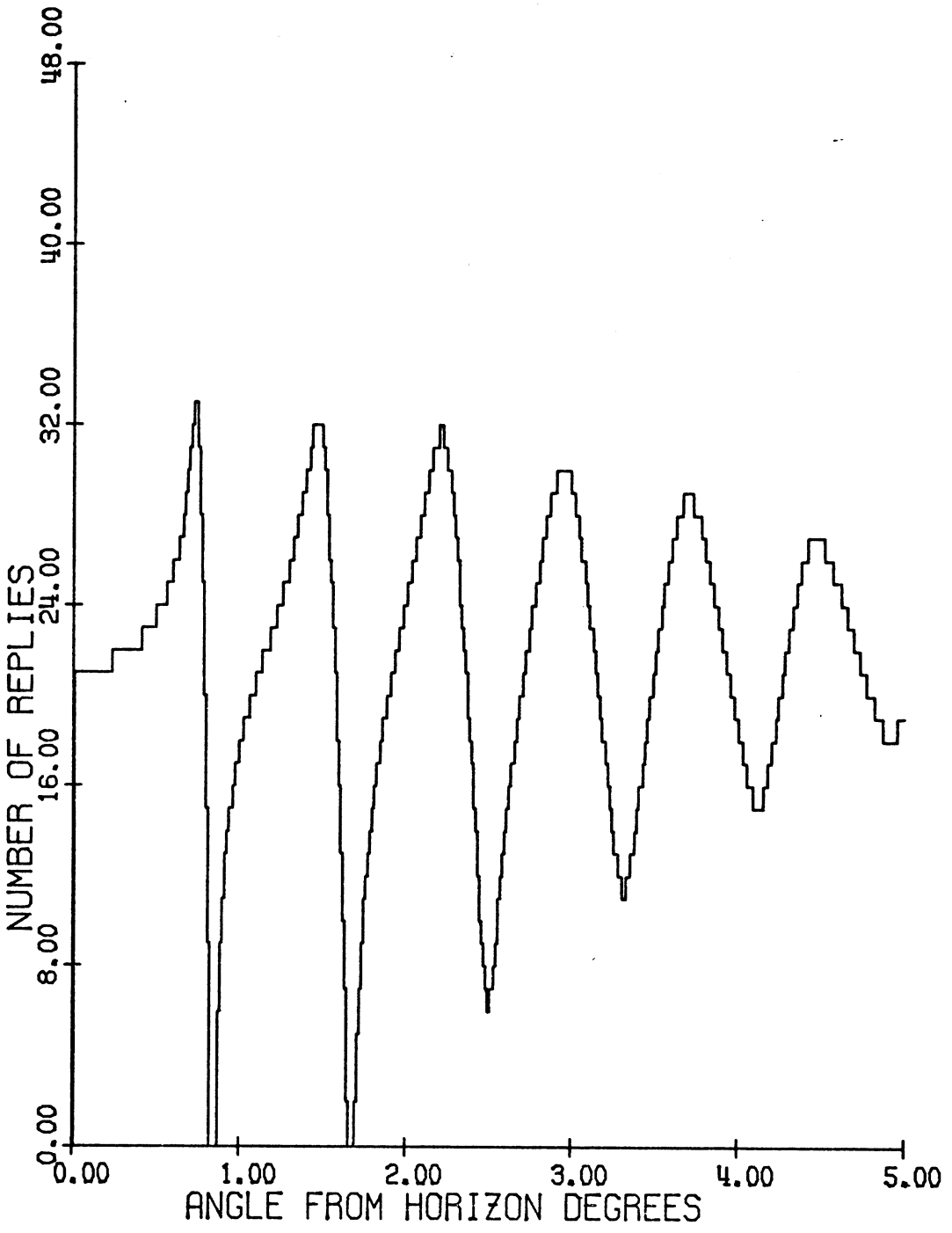

FIG. 9(a): Number of replies as a function of θ for the Hazeltine antenna. $\epsilon_r = 3$, PRF = 400, RPM = 12.6.

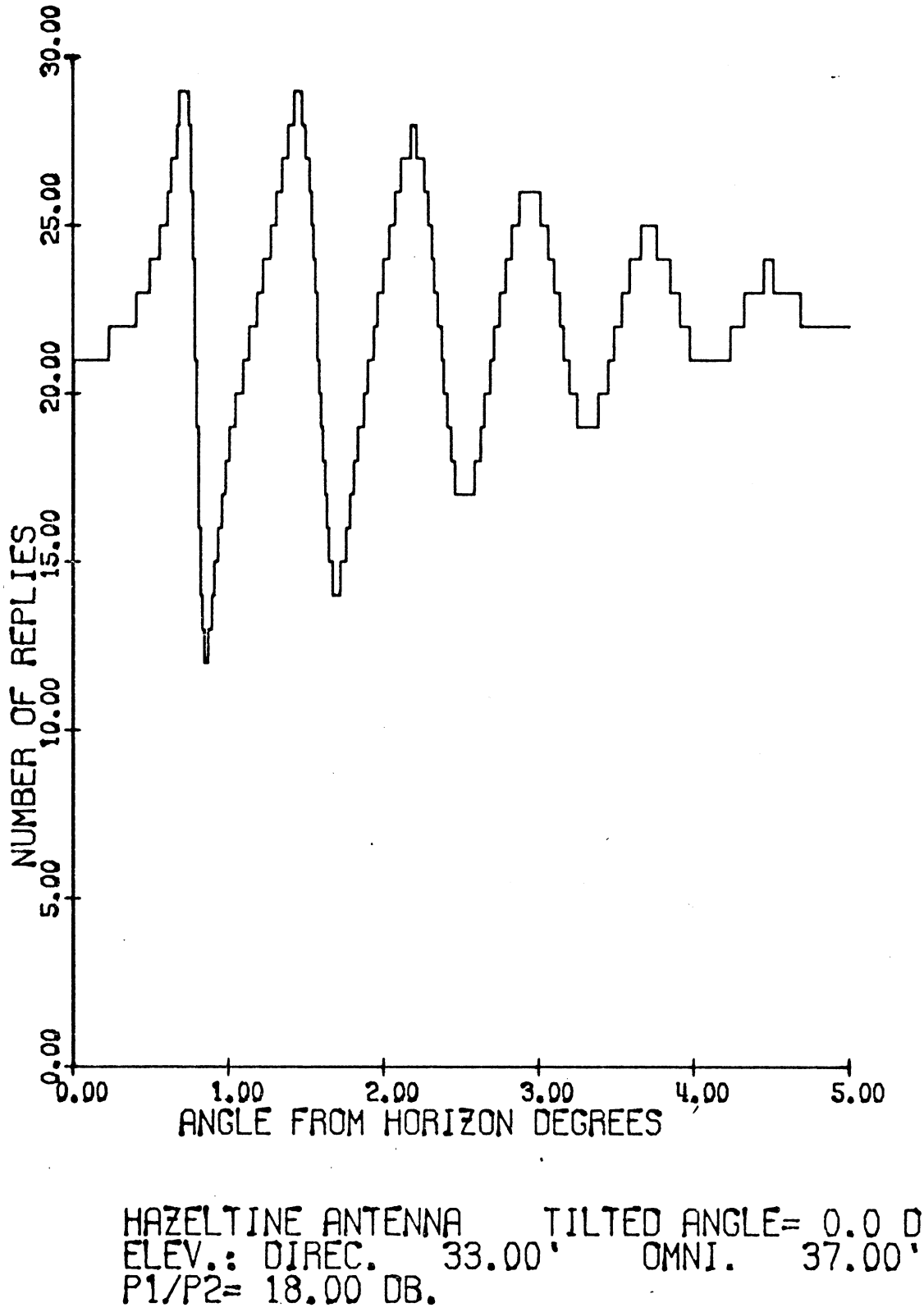

FIG. 9(b): Number of replies as a function of θ for the Hazeltine antenna. $\epsilon_r = 80.0$, PRF = 400, RPM = 12.6.

effects of the increased dielectric constant are found to be that the number of replies does not go to zero and that it approaches the free space value of 22 more quickly.

The coverage diagrams for the antenna are shown in Figs. 10(a) and 10(b) for $\epsilon_c = 3.0 - j0.0$ and $80 - j0.00$ respectively. It is assumed that the maximum free space range is 100 nautical miles at $\theta \sim 13^o$. Appreciable amounts of fluctuations in coverage around the free space value continue up to $\theta \sim 10^o$ for $\epsilon_c = 3.00 - j0.00$ and to $\theta \sim 7^o$ for $\epsilon_c = 80.0 - j0.0$. Beyond these angles the coverage patterns approximately follow the free space pattern. The smoothing effects of the large dielectric constant are also evident in the results shown. The results indicate that the locations of the maxima and minima in the coverage diagrams, particularly in the region near the horizon, are approximately the same for the two cases. For the height of the antenna they occur at angles approximately 0.8^o apart. The first maximum and minimum occur at $\theta \sim 0.4^o$ and $\theta \sim 0.8^o$ respectively. The ranges at the first 3 maxima are about 99, 96, and 95 nautical miles for $\epsilon_c = 3 - j0.00$ and 96, 91 and 87 nautical miles for $\epsilon_c = 3.0 - j0.00$ and 20, 36 and 48 nautical miles for $\epsilon_c = 80 - j0.00$ respectively. The large dielectric constant is thus found to increase significantly the ranges at the first few minima.

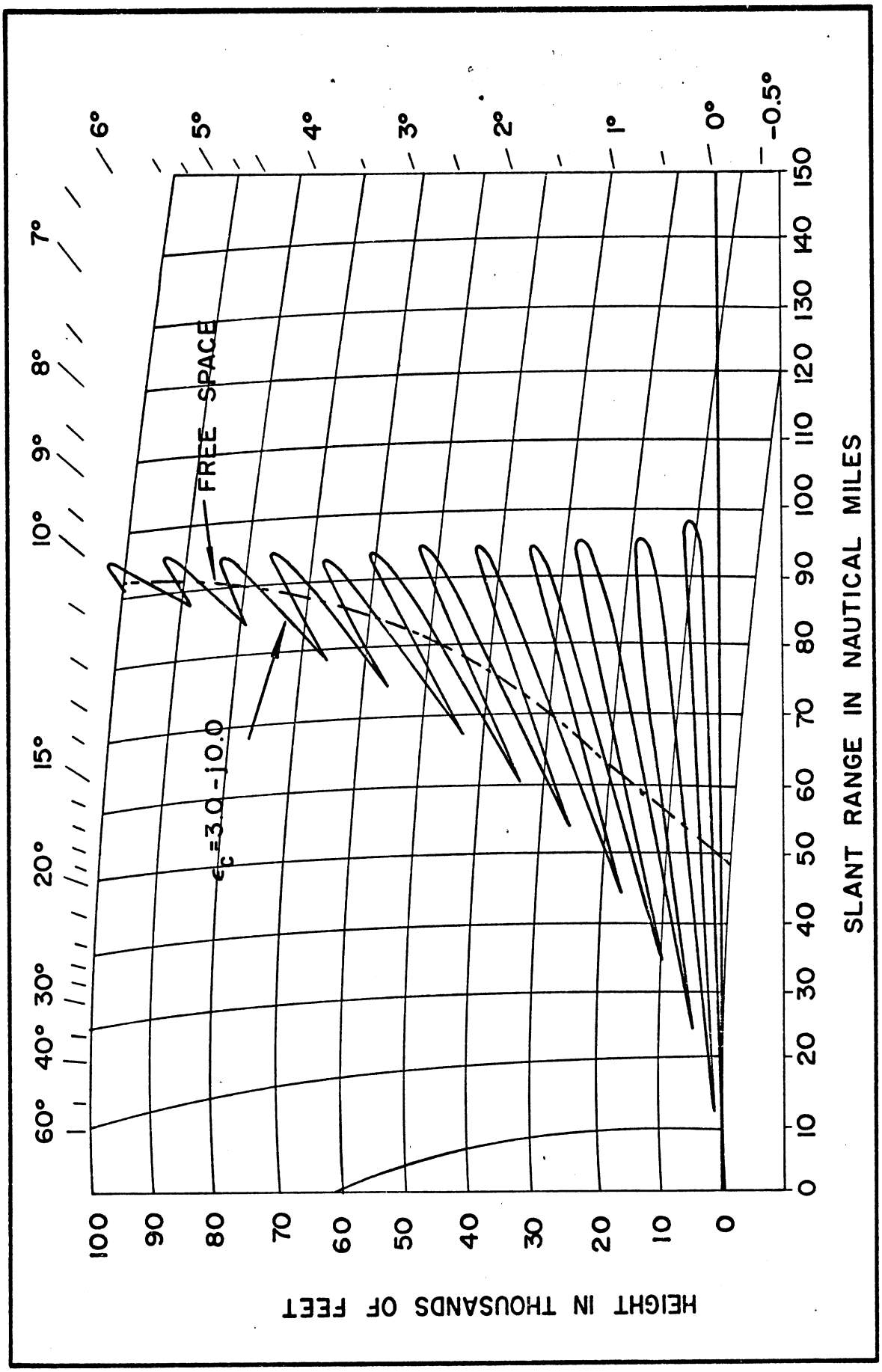

FIG. 10(a): Coverage diagram for the Hazeltine antenna for ϵ_c = 3.0-j0.0. Maximum free space range is 100 nautical miles.

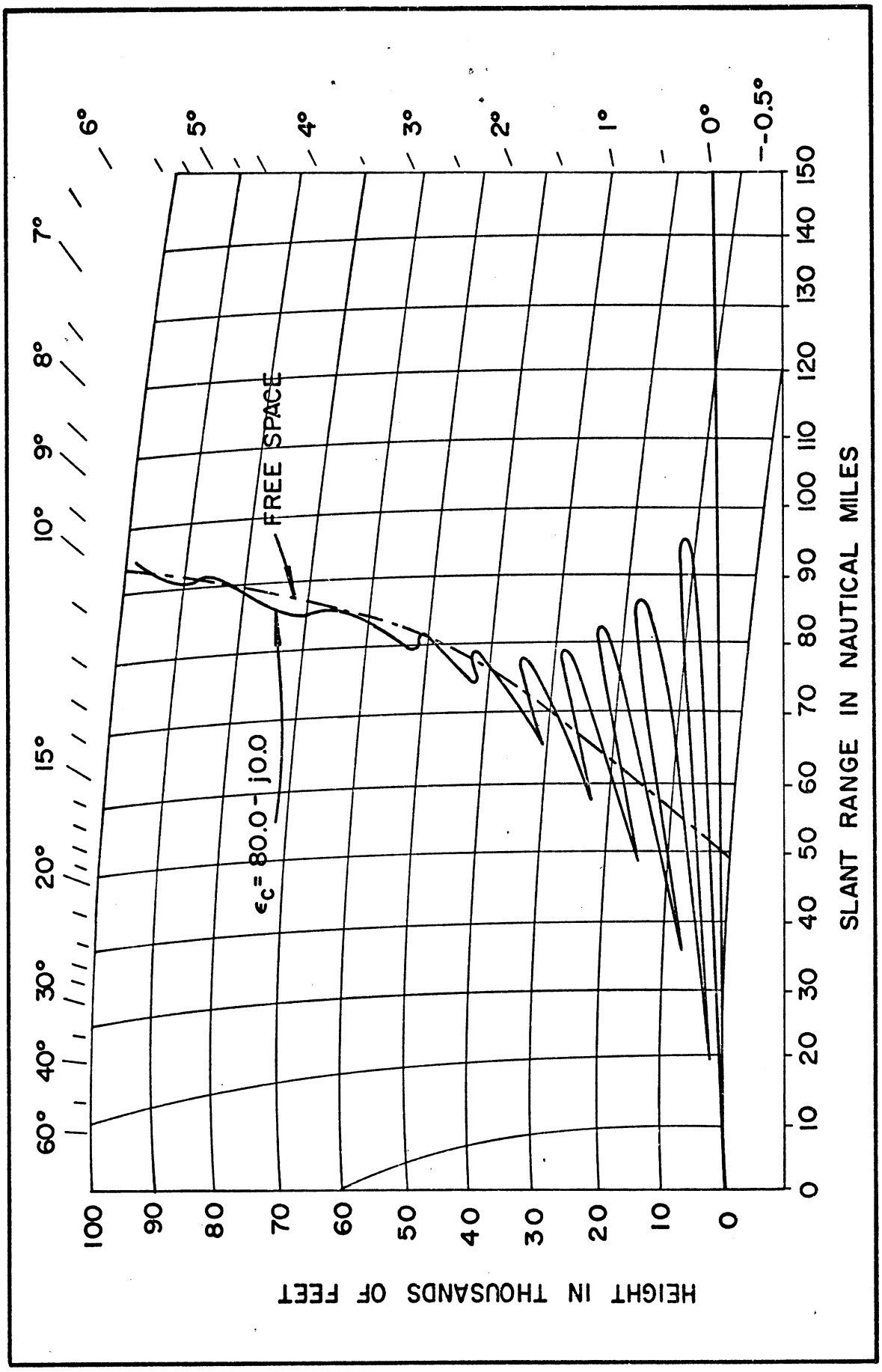

Fig. 10(b): Coverage diagram for the Hazeltine antenna for ϵ_c = 80.0-j0.0. Maximum free space range is 100 nautical miles.

5. RESULTS FOR THE EXISTING (HOG-TROUGH) ANTENNA

Figures 11(a) and 11(b) show that in the SLS mode P1 and P2 pulse patterns obtained with the existing antenna located above a flat ground having $\epsilon_c = 3.0 - j0.0$, a peak-to-peak fluctuation of 2 dB around the free space value is reached at $\theta \sim 20^o$ whereas for $\epsilon_c = 80.0 - j0.0$ the first 2 dB peak-to-peak fluctuation point is reached at $\theta \sim 5^o$.

It should be noted that the critical angle for $\epsilon_c = 80.0 - j0.0$ is at $\theta = \theta_B = 6^o22'$ where the reflection coefficient is zero, and beyond $\theta > \theta_B$ it increases (see Fig. 3) at first rapidly and then slowly to a maximum value of about 0.8. The effects of this may be seen distinctly in Fig. 11(b) where it is found that P1 and P2 pulse patterns assume their respective free space values around θ $\theta_B = 6^o22'$ and the fluctuation amplitudes around the free space values slowly increase for $\theta > \theta_B$. The corresponding patterns shown in Fig. 4(b) for the Hazeltine antenna do not show these effects because of the fact that it has a larger field gradient. Fig. 12 shows the P1 and P2 pulse patterns in the range $0 \leq \theta \leq 5^o$ on an expanded scale and for $\epsilon_c = 3.0 - j0.0$ and $80.0 - j0.0$. The smoothing effects of the large dielectric constant can be seen in the results shown.

The normalized pulse ratio patterns for $\epsilon_c = 3.0 - j0.0$ and $80.0 - j0.0$ are shown in Figs. 13(a) and 13(b) respectively. It is found that the large dielectric constant tends to smooth out quite strongly the overall fluctuations of P1/P2 as a function of θ. As far as the mainbeam killing and sidelobe punch-through phenomena are concerned, the results in Figs. 13(a) and 13(b) show the dramatic reduction of such effects by the medium with large dielectric constant.

The behavior of the P1/P2 patterns in Figs. 13(a) and 13(b) (also in Figs. 6(a) and 6(b)) resembling the familiar beating phenomenon between two harmonic waves needs some explanation. The P1/P2 ratio envelope will assume zero value at the critical angle, defined earlier, where there exists no reflected wave and also at angles where the P1 and P2 patterns align with each other and with their corresponding free space values. In the present case the latter angles may be referred to as the beating angles. The critical angles of $\epsilon_r = 3$ and 80 occur at 30^o and $6^o22'$ respectively; thus in Fig. 13(a) the critical angle is beyond the range shown and in Fig. 13(b) P1/P2 assumes zero value at $6^o22'$ as it should. It can be shown that the beating angles are determined by the separation between the phase centers of the directional and omnidirectional antennas and are given by:

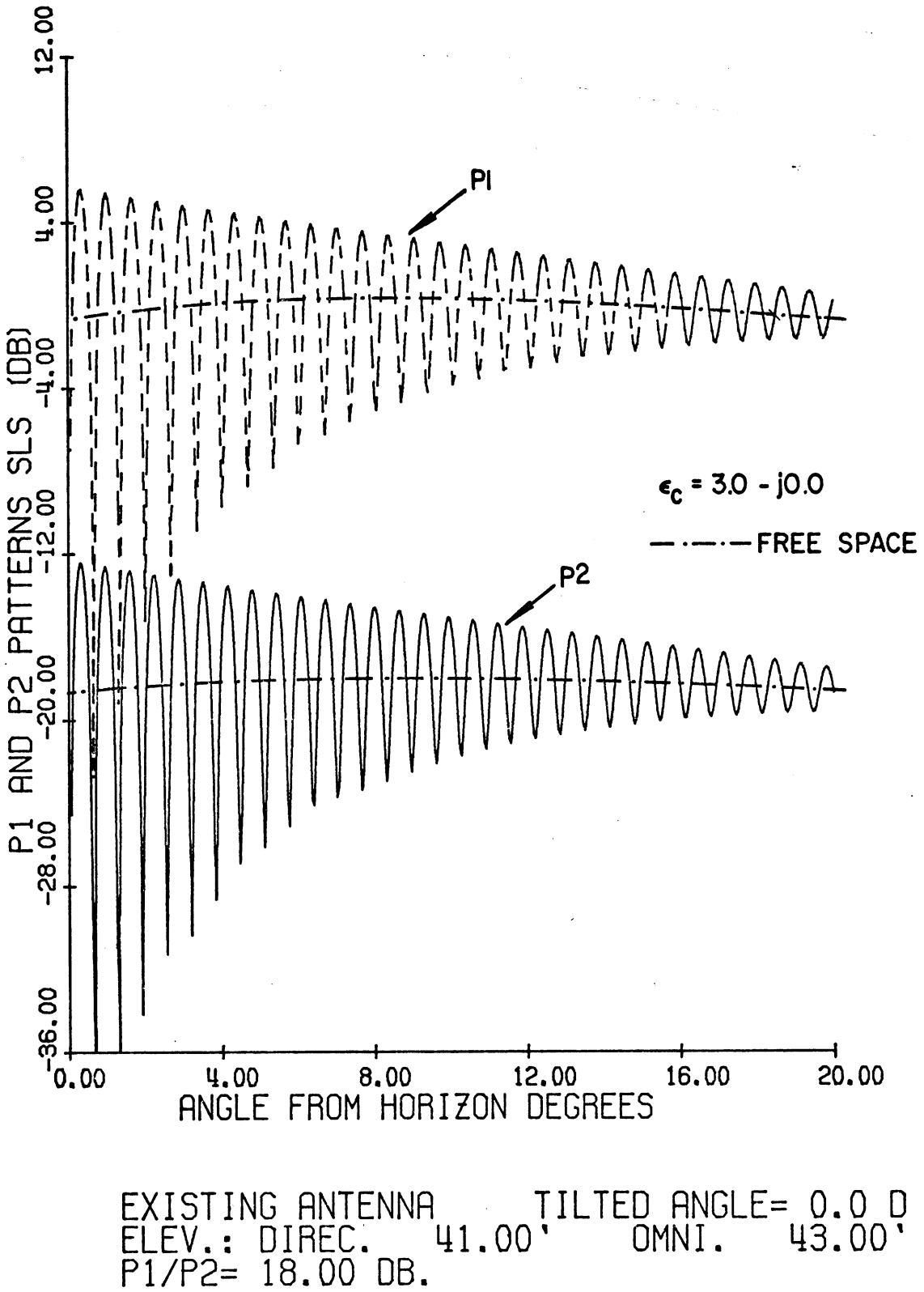

FIG. 11(a): SLS mode P1 and P2 pulse patterns for the existing Hog-trough antenna. $\epsilon_r = 3.0$.

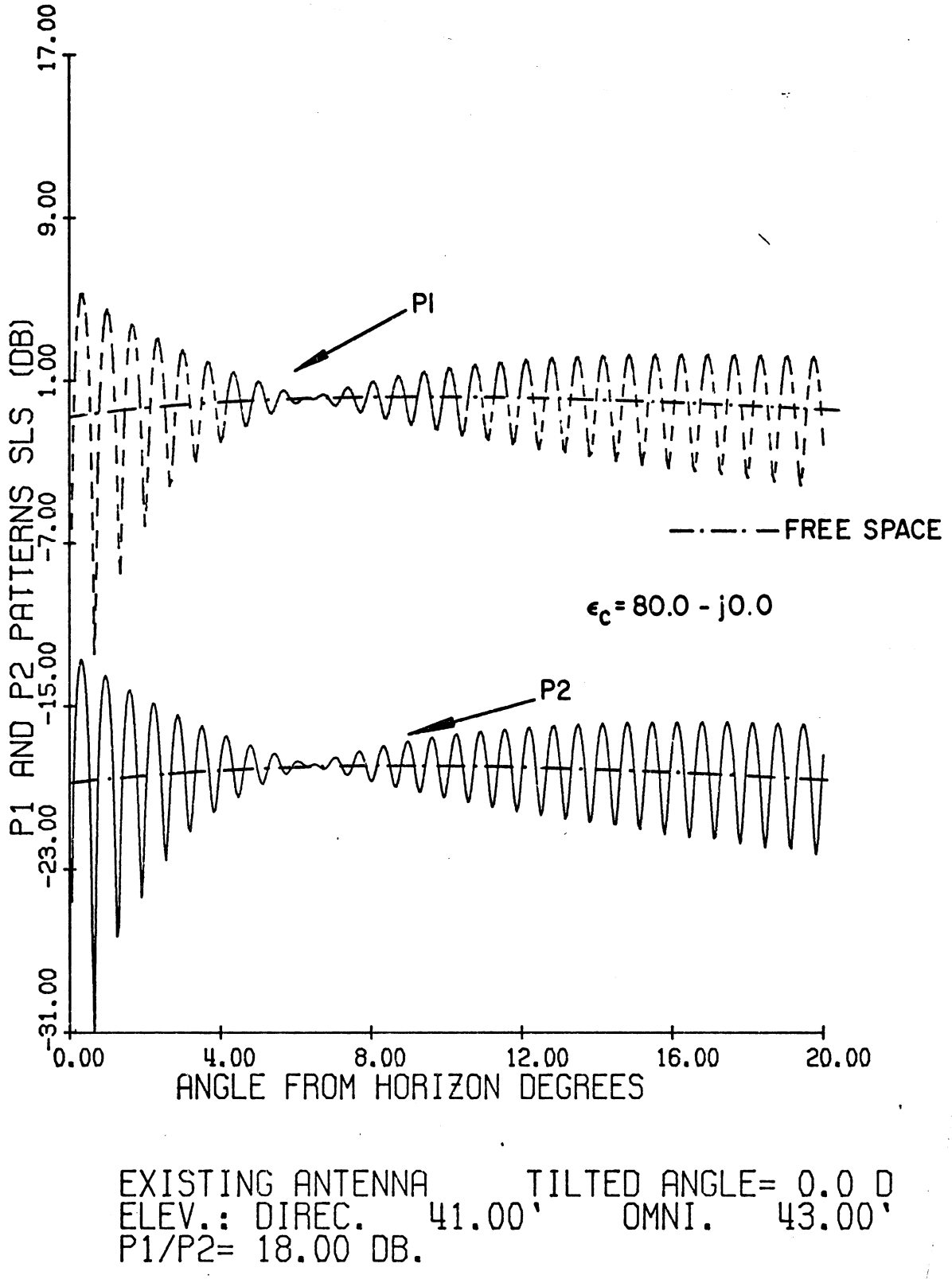

FIG. 11(b): SLS mode P1 and P2 pulse patterns for the existing Hog-trough antenna. $\epsilon_r = 80.0$.

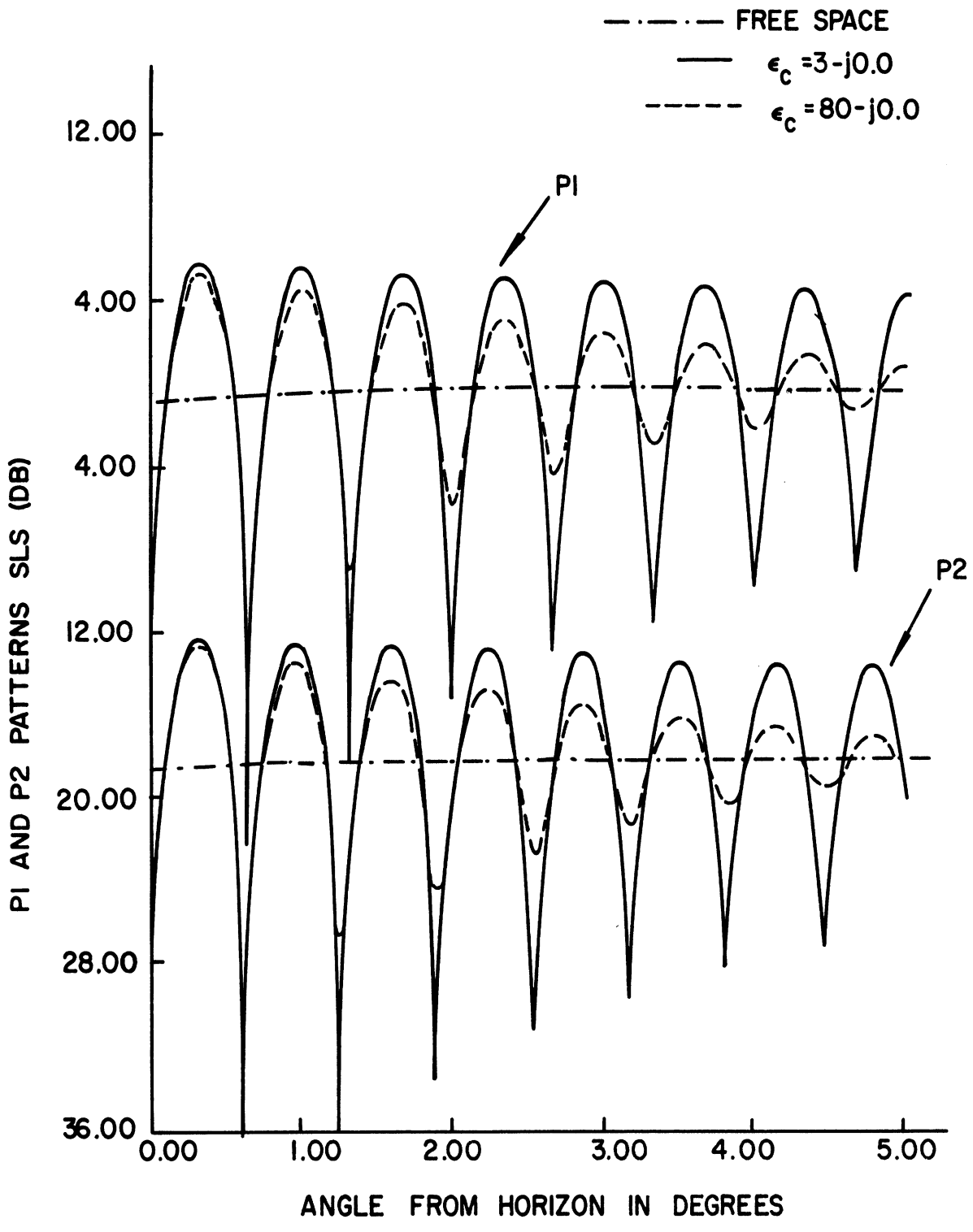

FIG. 12: SLS mode P1 and P2 pulse ratio patterns on expanded scale for the existing Hog-trough antenna.

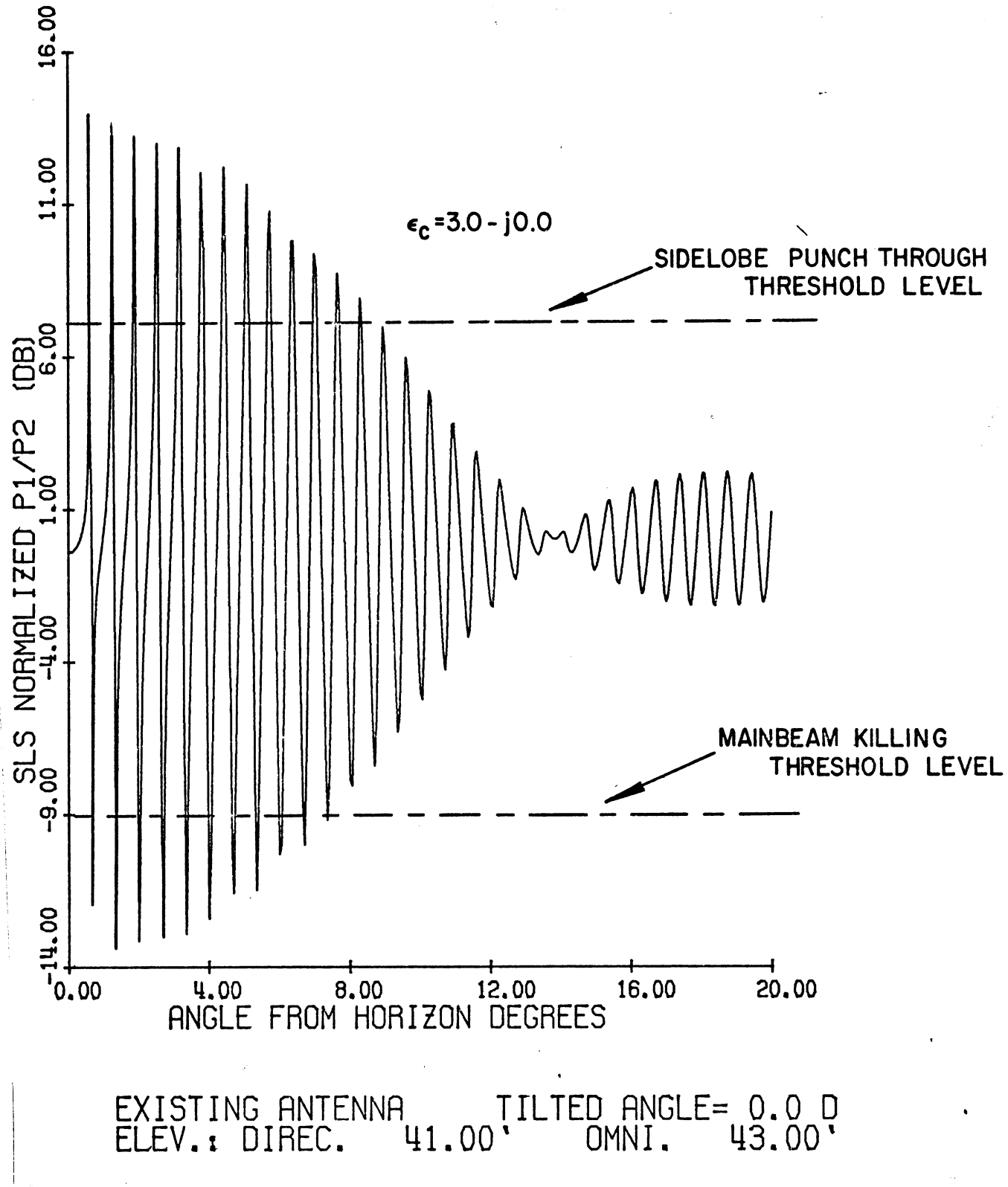

FIG. 13(a): SLS mode normalized pulse ratio pattern for the existing Hog-trough antenna. $\epsilon_r = 3.0$.

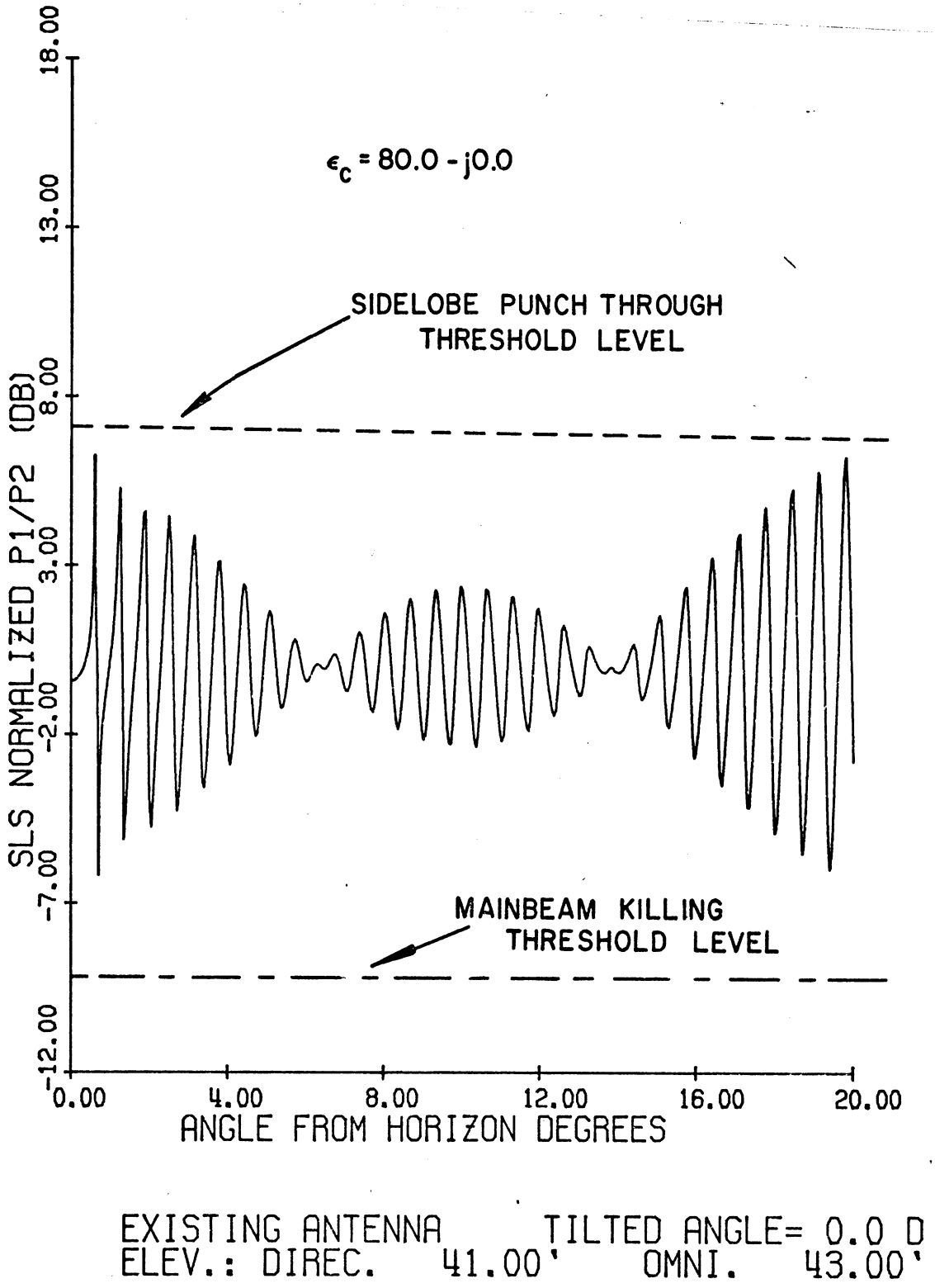

FIG. 13(b): SLS mode normalized pulse ratio pattern for the existing Hog-trough antenna. $\epsilon_r = 80.0$.

$$\sin\theta'_r \simeq -\frac{n\lambda}{2(H_o - H_d)} \quad , n = 1, 2, \ldots, \qquad (4)$$

where,

H_o is the height of the phase center of the omnidirectional antenna located above ground,

H_d is the height of the phase center of the directional antenna located above ground,

λ is the force space wavelength.

In the present case, for the existing Hog-trough antenna $H_o - H_d \simeq 2'$ and $\lambda \simeq 1'$ and the first beating angle occurs at $\theta'_1 \simeq 14^o15'$which is also the angle at which P1/P2 = 0 in Figs. 13(a) and 13(b). The beating effects may be controlled to a certain extent by adjusting the separation distance between the two antennas. Figs. 14(a) and 14(b) show the normalized pulse ratio pattern for the existing Hog-trough antenna with two different values of the separation between the phase center of the two antennas. On comparing Figs 13 and 14 is may be said that the numbers of mainbeam killings and sidelobe punch-through zones in space for a given initerrogator antenna system may be reduced by increasing the separation distance between the phase centers of the two antennas.

Figures15(a)and 15(b) show the number of replies as a function of θ within in range $0 \leq \theta \leq 5^o$for $\epsilon_c = 3.0 - j0.0$ and $80.0 - j0.0$ respectively. Within the range of θ considered in Fig. 15, the number of replies goes to zero 7 times for $\epsilon_c = 3.0 - j0.0$ whereas for $\epsilon_c = 80.0 - j0.0$, it always stays above zero. Appreciable fluctuations in the number of replies continue up to $\theta = 20^o$, where the number of replies is 16 for $\epsilon_c = 3.0 - j0.0$. For $\epsilon_c = 80.0 - j0.0$ the number of replies assumes the free space value of 15 in the region near the critical angle $\theta_B \sim 6^o22'$; for $\theta > \theta_B$ the number of replies fluctuates slightly up to $\theta = 20^o$ where it assumes a value of 15.

The coverage diagrams for the Hog-trough antenna are shown in Figs. 16(a) and 16(b) for $\epsilon_c = 3.0 - j0.0$ and $80.0 - j0.0$ respectively. It is assumed that the maximum free space range is 100 nautical miles which occurs at $\theta \sim 3.9^o$. For $\epsilon_c = 3.0 - j0.0$, an appreciable amount of lobing in the coverage diagram continues up to about $\theta \sim 20^o$. For $\epsilon_c = 80.0 - j0.00$, large fluctuations of the covrage around the free space value

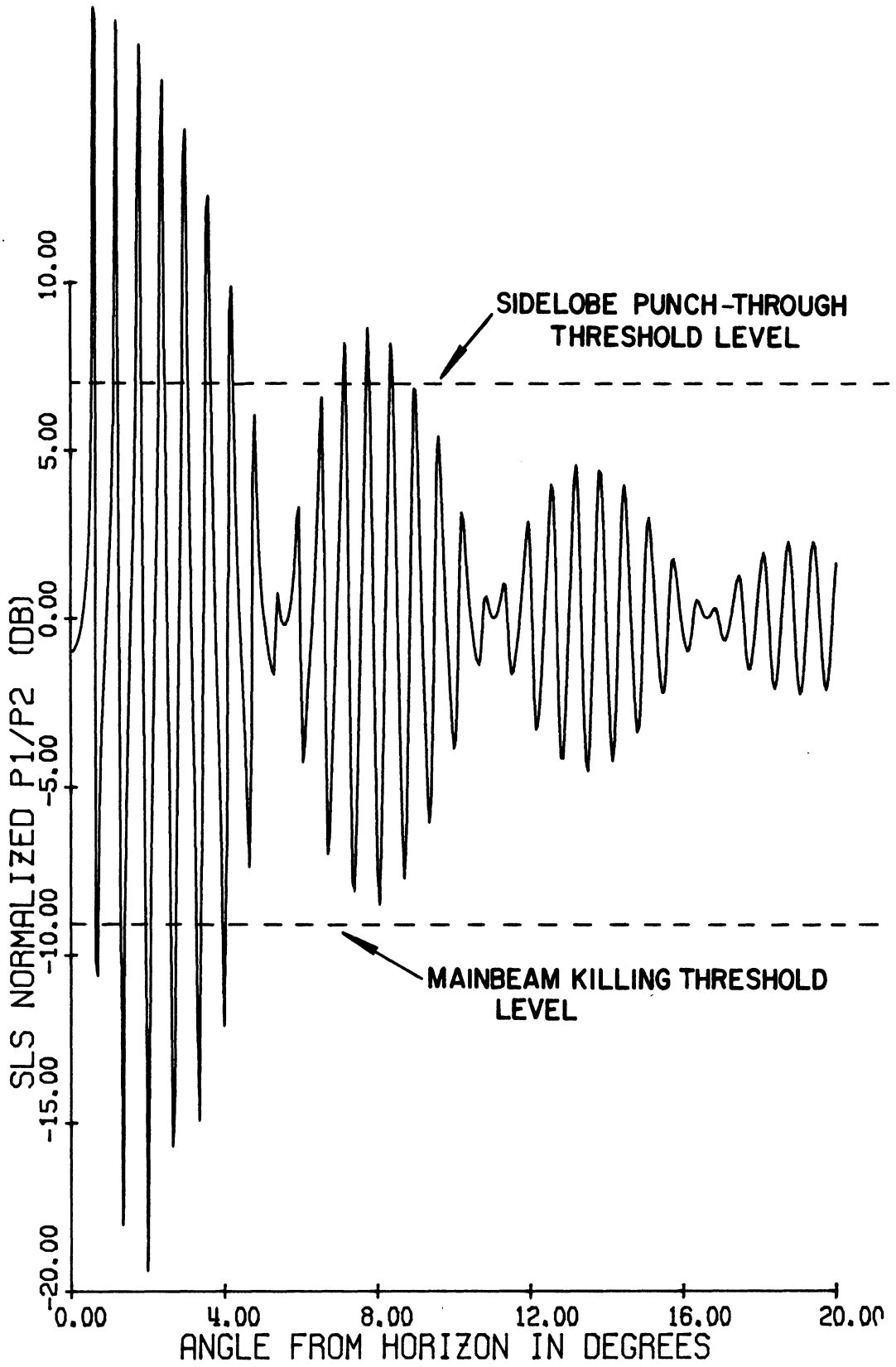

Fig. 14(a): SLS mode normalized pulse ratio pattern for the existing Hog-trough antenna. $\epsilon_r = 3.0$, $H_o - H_d = 3'$.

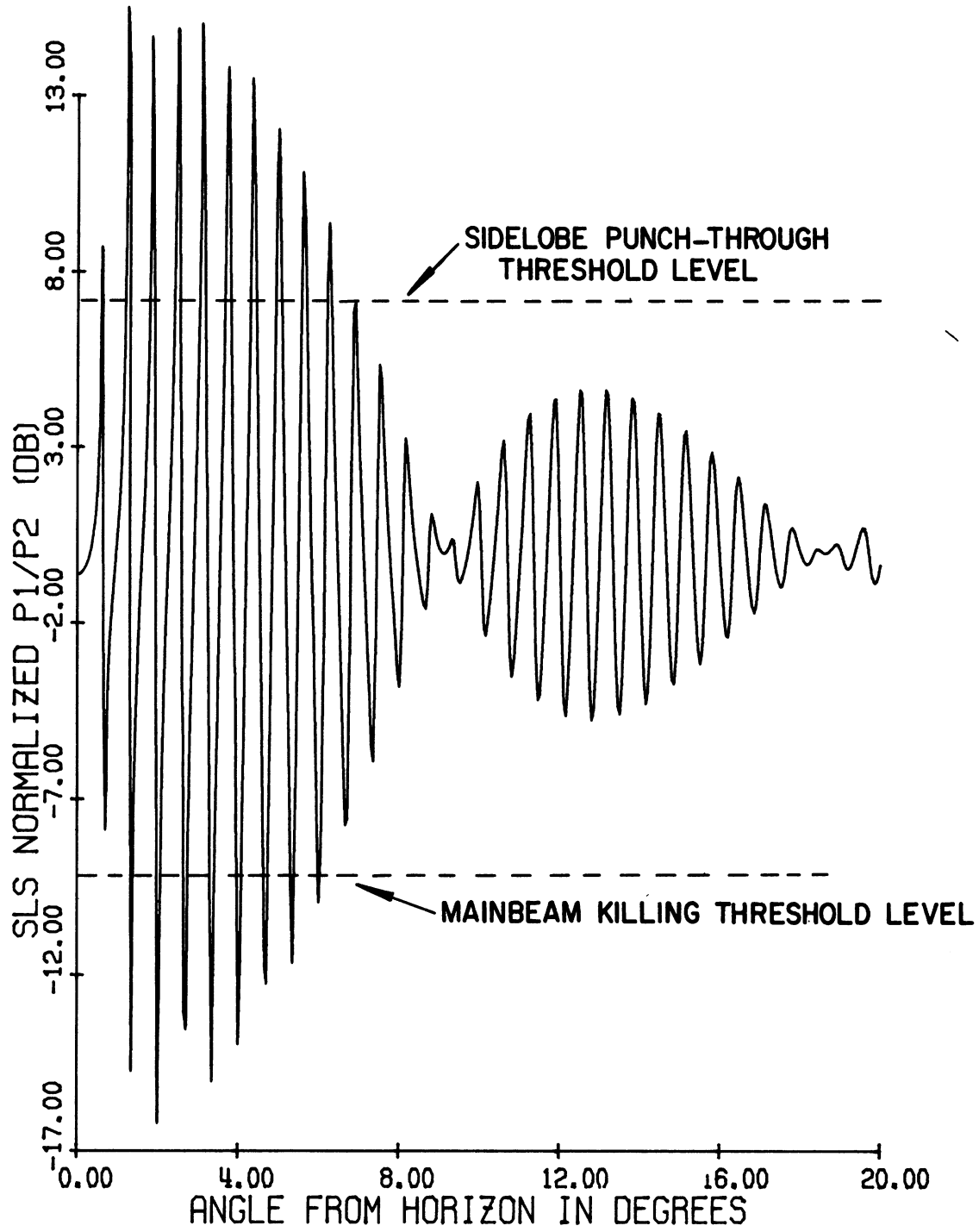

Fig. 14(b): SLS mode normalized pulse ratio pattern for the existing Hog-trough antenna. $\epsilon_r = 3.0$, $H_o - H_d = 5'$.

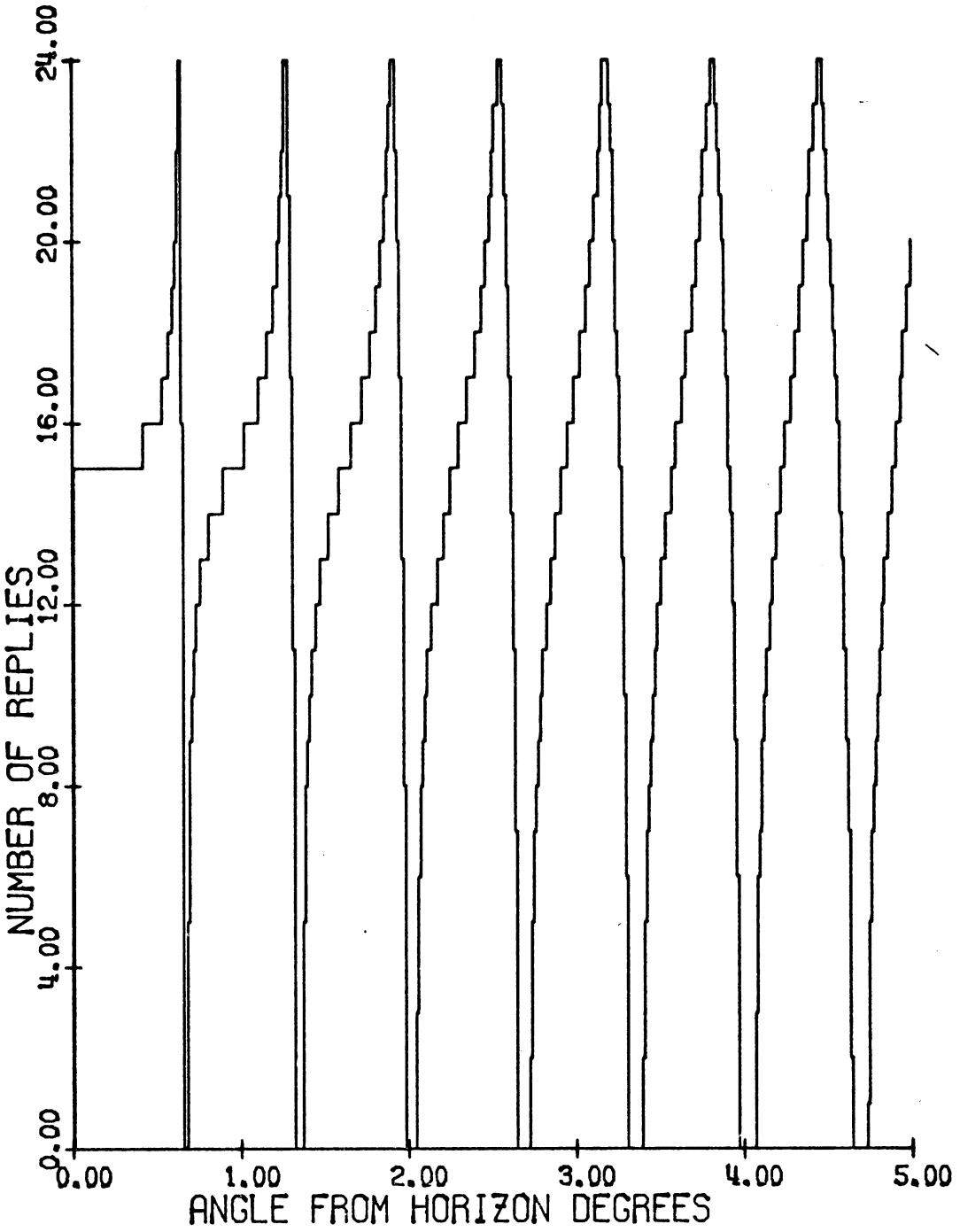

FIG. 15(a): Number of replies as a function of θ for the existing Hog-trough antenna. $\epsilon_r = 3$, PRF = 360, RPM = 15.

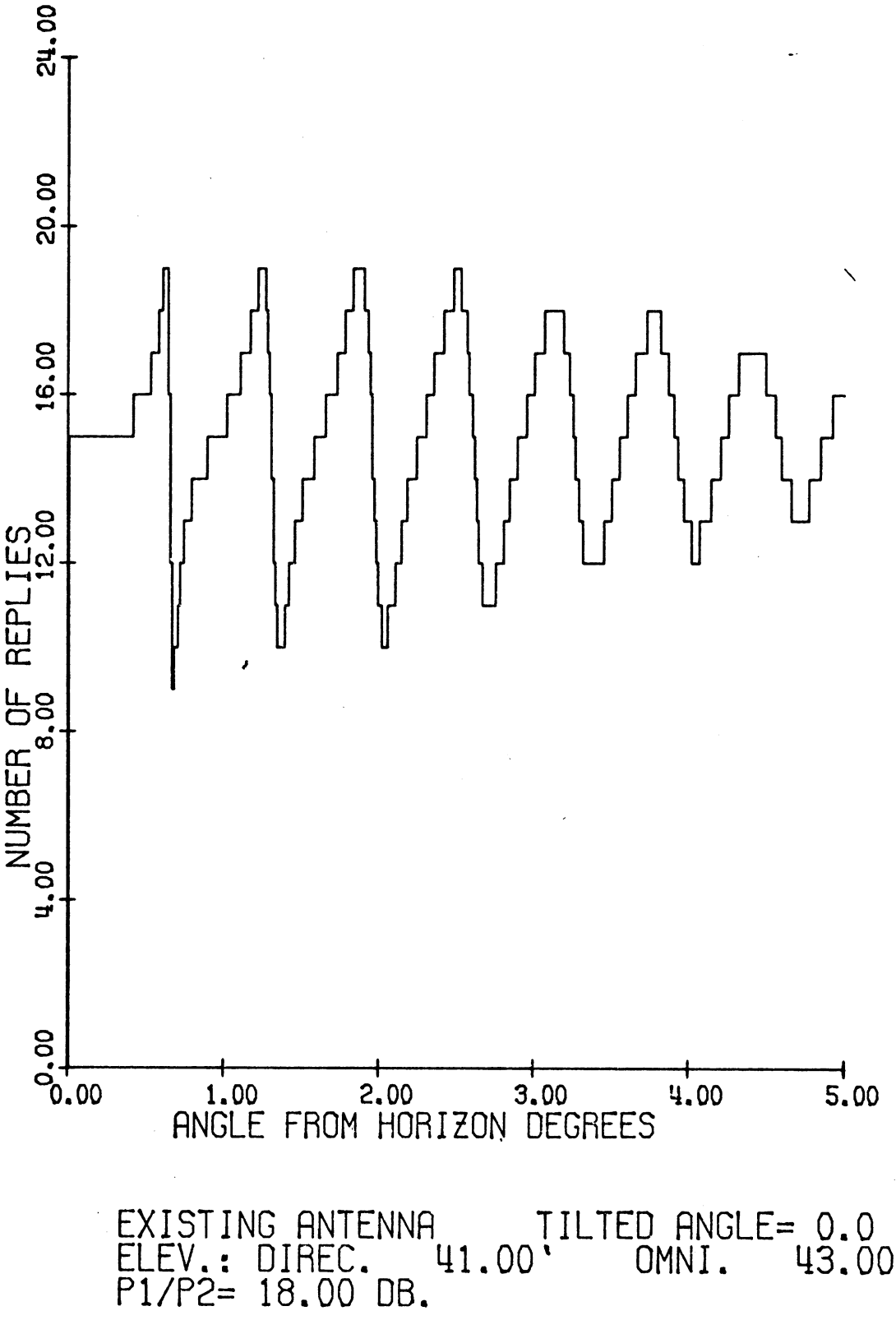

FIG. 15(b): Number of replies as a function of θ for the existing Hog-trough antenna. $\epsilon_r = 80.0$, PRF = 360, RPM = 15.

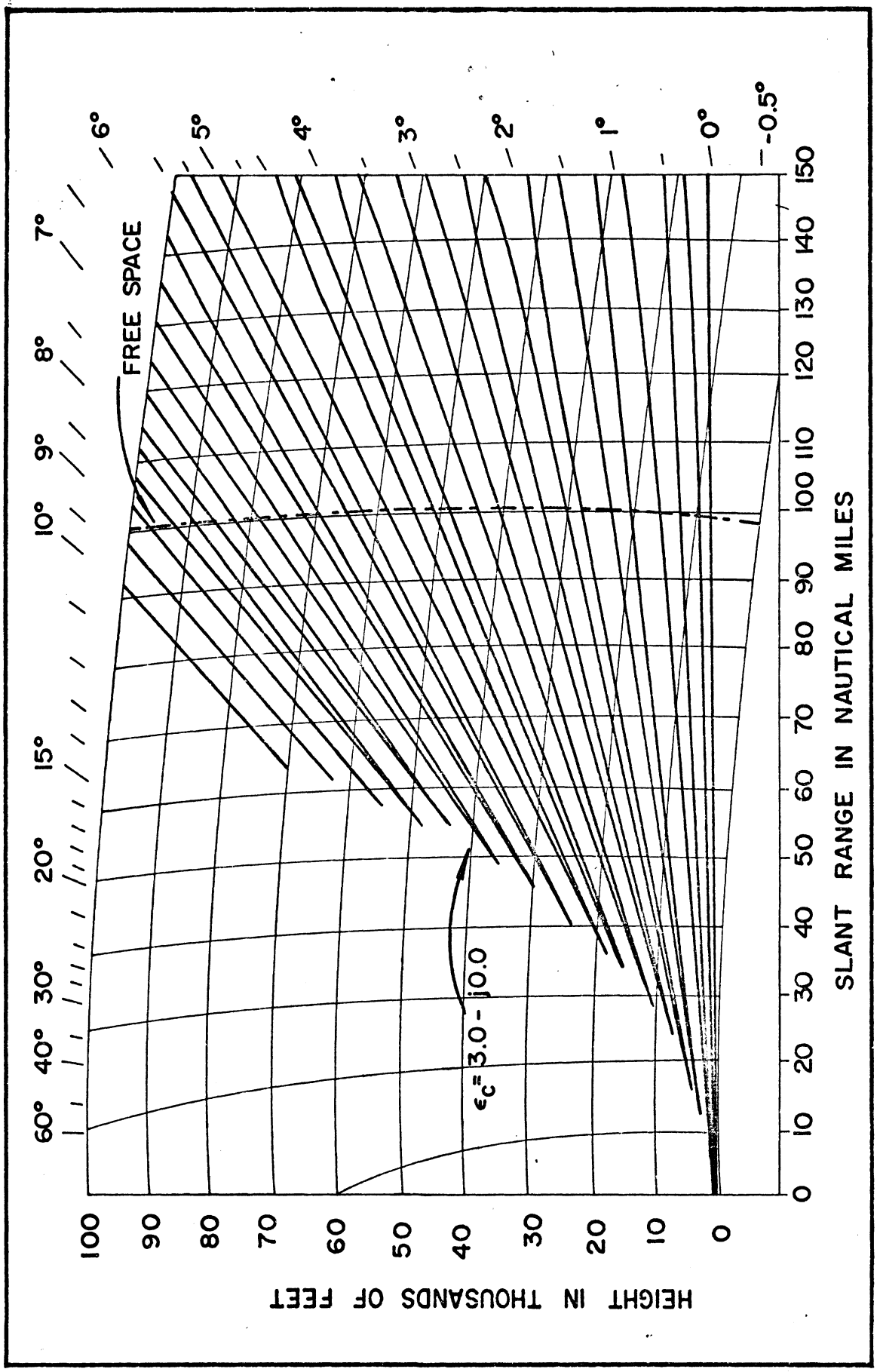

FIG. 16(a): Coverage diagram for the existing Hog-trough antenna. $\epsilon_r = 3.0$. Maximum free space range is 100 nautical miles.

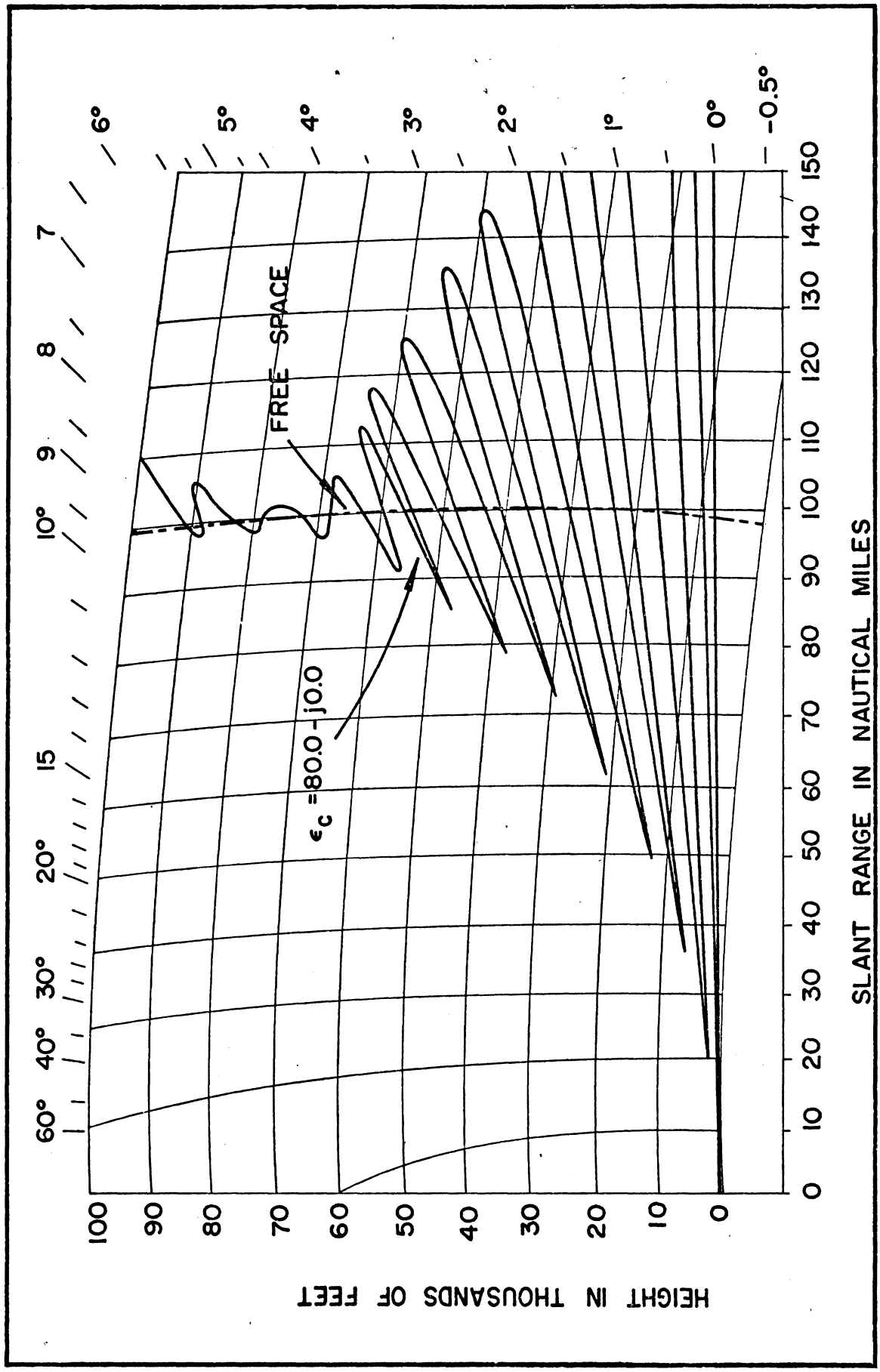

FIG. 16(b): Coverage diagram for the existing Hog-trough antenna. $\epsilon_r = 80.0$. Maximum free space range is 100 nautical miles.

continue up to the critical angle region $\theta_B \sim 6^o$ where the coverage assumes the free space value. Beyond $\theta > \theta_B$ the lobing tends to increase again. The smoothing effects of the large dielectric constant are found to be quite strong. For the given height of the antenna, the maxima and the minima in the coverage diagrams occur at about 0.65^o apart; the first maximum occurs at $\theta \quad 0.34^o$ and the first minimum occurs at $\theta \sim .66^o$. The ranges at the first 3 minima are 7, 12 and 17 nautical miles for $\epsilon_c = 3.0 - j0.0$ and 20, 36 and 49 nautical miles for $\epsilon_c = 80.0 - j0.00$ respectively. The increases in the ranges at low angles for the larger dielectric constant case are quite significant At large angles, say θ in the range $10^o \leq \theta \leq 20^o$, the advantage of the smoothing effects of the large dielectric constant are lost.

6. COMPARISON OF RESULTS

It is of interest to compare the performance of ATCRBS using the two antennas as the dielectric constant of the ground is varied. An important parameter which determines the ATCRBS performance is the peak-to-peak fluctuations around the free space values in the P1 and P2 pulse patterns. Figure 17 shows the variation with dielectric constant of the angle of the maximum which is 2 dB above the previous adjacent minimum in the P1 pulse patterns of the two antennas. In general, this angle at first decreases rapidly with ϵ_r at the lower end and then slowly at the larger end. For small values of ϵ_r the existing antenna is found to be considerably more sensitive to the variation of ϵ_r.

The mainbeam killing and sidelobe punch-through zones in space are determined by whether the maxima and minima in the P1/P2 patterns cross the respective threshold levels. It is therefore of interest to study the effects of dielectric constant on the levels of the maxima and minima in the P1/P2 patterns. As indicated earler, the effects are most significant in the first few maxima and minima. Figure 18 shows the reduction in amplitude of the first maximum and in the depth of the first minimum in the P1/P2 patterns of the two antennas as functions of the dielectric constant. Again it is found that the variations are larger for small values of ϵ_r and that the existing antenna is significantly more sensitive to the variations of ϵ_r.

With respect to the coverage diagrams, the same comment applies to the existing antennas.

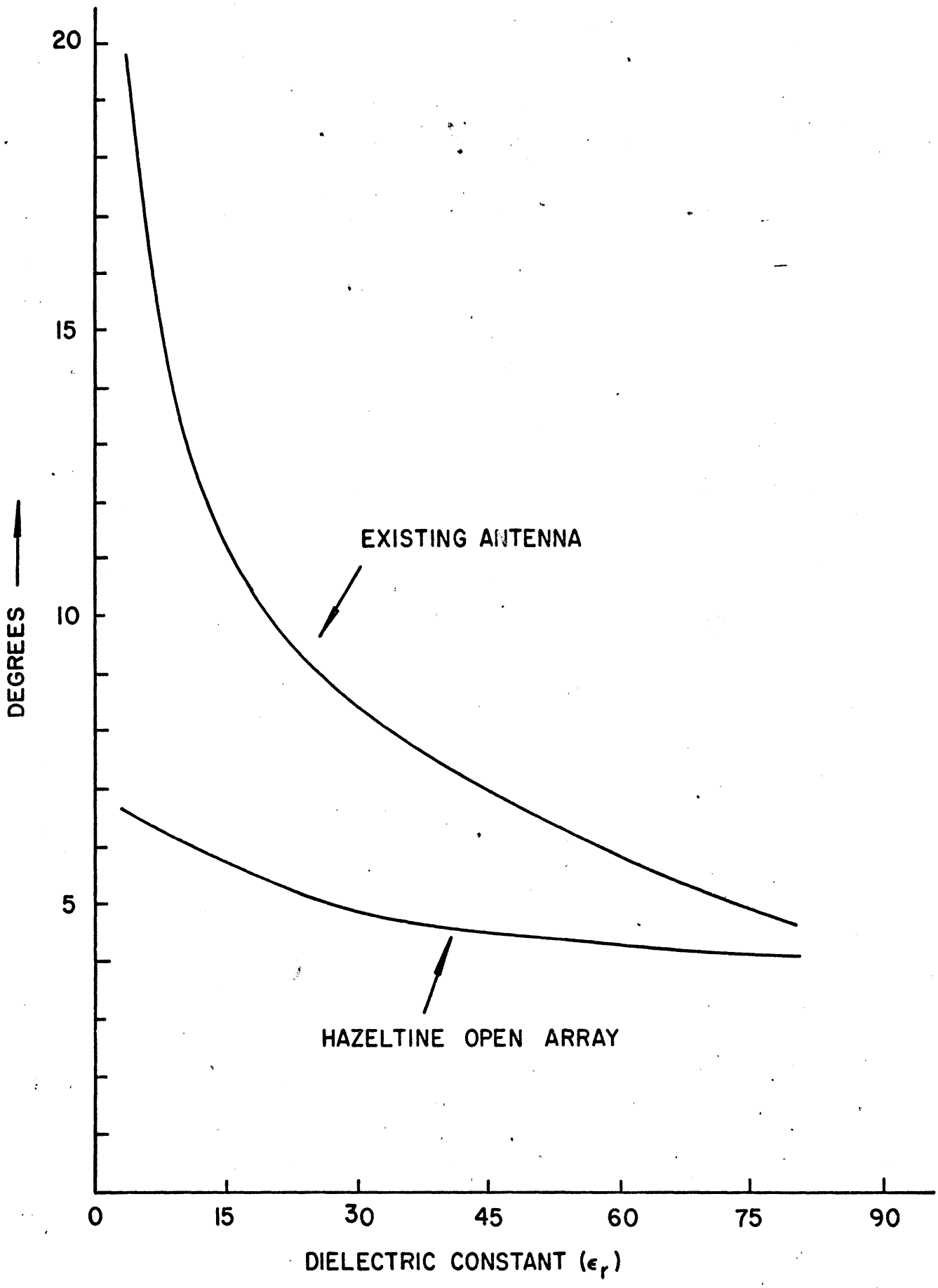

FIG. 17: The variation with dielectric constant of the angle of the maximum which is 2 dB above the previous adjacent minimum in the P2 pattern.

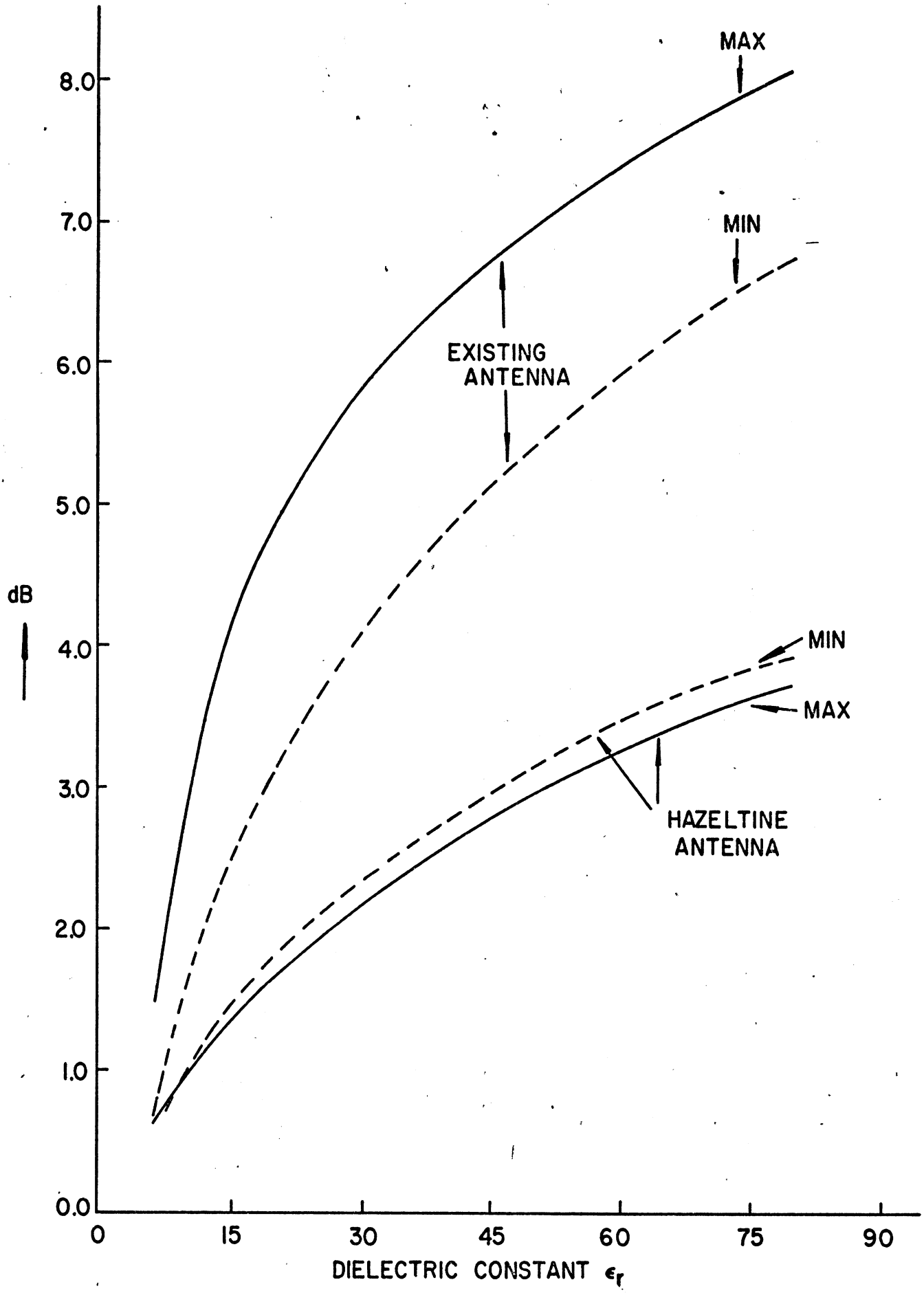

FIG. 18: Reduction in the amplitude of the first maximum and in the depth of the first minimum in the SLS mode pulse ratio pattern (P1/P2).

7. CONCLUSIONS

The SLS mode performance of ATCRBS located above a flat ground having variable dielectric constant has been discussed. On the basis of this investigation the following observations can be made:

(i) At the ATCRBS frequencies, the effects of the ground loss may be neglected in most of the cases.

(ii) Increase of the dielectric constant tends to smooth out the fluctuations of the characteristic quantities around the free space values.

(iii) The existing antenna is found to be more sensitive to the variations of the dielectric constant. This implies that antennas with large field gradient will be less sensitive to the dielectric constant variations of the ground, i.e. to the changes in the ground constants due to weather effects.

(iv) The numbers of mainbeam killing and sidelobe punch-through zones for a given antenna system may be reduced slightly by increasing the separation distance between the phase centers of the two antennas.

8. REFERENCES

1 J. Zatkalik, D. L. Sengupta and C. T. Tai, "Side Lobe Suppression Mode Performance of ATCRBS with Various Antennas", FAA-RD-75-31, May 1975.

2 D. L. Sengupta, J. Zatkalik and C. T. Tai, "Improved Side Lobe Suppression Mode Performance of ATCRBS with Various Antennas", FAA-RD-75-32, May 1975.

3 D. L. Sengupta and J. Zatkalik, "A Theoretical Study of the SLS and ISLS Mode Performance of Air Traffic Control Radar Beacon System", Record of the IEEE 1975 International Radar Conference, published by IEEE AES, New York, pp. 132-137.

4 D. E. Kerr, "Propagation of Short Radio Waves, Boston Technical Publishers, Inc., Mass., 1964, Chapter 5.

5 E. C. Jordan and K. G. Balmain, Electromagnetic Waves and Radiating Systems, 2nd Ed., Printice-Hall, Inc., New Jersey, 1968, pp. 628-635.

6 G. F. Spingler, "Experimentation and Analysis of Siting Criteria", Report No. NA-69-36 (RD-69-43), Project No. 242,-001-05X, FAA, NAFEC, Atlantic City, New Jersey, September 1969.

7 F. LaRussa, Private communication, 1974.